



1 **Using flow cytometry and light-induced fluorescence technique to characterize the**  
2 **variability and characteristics of bioaerosols in springtime at Metro Atlanta, Georgia**

3  
4 Arnaldo Negron<sup>a,b</sup>, Natasha DeLeon-Rodriguez<sup>c§</sup>, Samantha M. Waters<sup>a#</sup>, Luke D. Ziemba<sup>d</sup>,  
5 Bruce Anderson<sup>d</sup>, Michael Bergin<sup>e</sup>, Konstantinos T. Konstantinidis<sup>f,c\*</sup>, and Athanasios  
6 Nenes<sup>a,b,g,h,i\*</sup>

7 <sup>a</sup> School of Earth and Atmospheric Sciences, Georgia Institute of Technology, Atlanta, GA 30332, USA

8 <sup>b</sup> School of Chemical and Biomolecular Engineering, Georgia Institute of Technology, Atlanta, GA  
9 30332, USA

10 <sup>c</sup> School of Biology, Georgia Institute of Technology, Atlanta, GA 30332, USA

11 <sup>d</sup> Chemistry and Dynamics Branch/Science Directorate, National Aeronautics and Space Administration  
12 Langley Research Center, Hampton, VA 23681, USA

13 <sup>e</sup> Department of Civil and Environmental Engineering, Duke University, Durham, NC, 2770, USA

14 <sup>f</sup> School of Civil and Environmental Engineering, Georgia Institute of Technology, Atlanta, GA 30332,  
15 USA

16 <sup>g</sup> Institute of Environmental Research & Sustainable Development, National Observatory of Athens, GR-  
17 15236, Greece

18 <sup>h</sup> Institute for Chemical Engineering Science, Foundation for Research and Technology Hellas, Patra,  
19 GR-26504, Greece

20 <sup>i</sup> Laboratory of Atmospheric Processes and their Impacts (LAPI), School of Architecture, Civil &  
21 Environmental Engineering, Ecole Polytechnique Fédérale de Lausanne, CH-1015, Switzerland

22 <sup>§</sup> Currently at: Puerto Rico Science, Technology and Research Trust, Rio Piedras, 00927, Puerto Rico

23 <sup>#</sup> Currently at: Department of Marine Sciences, University of Georgia, Athens, GA 30602-3636

24 \*Corresponding Author

25 **Abstract**

26 The abundance and speciation of primary biological aerosol particles (PBAP) is important for  
27 understanding their impacts on human health, cloud formation and ecosystems. Towards this, we have  
28 developed a protocol for quantifying PBAP collected from large volumes of air with a portable wet-walled  
29 cyclone bioaerosol sampler. A flow cytometry (FCM) protocol was then developed to quantify and  
30 characterize the PBAP populations from the sampler, which were confirmed against epifluorescence  
31 microscopy. The sampling system and FCM analysis were used to study PBAP in Atlanta, GA over a two-  
32 month period and showed clearly defined populations of DNA-containing particles: Low Nucleic Acid-  
33 content particles (bioLNA), High Nucleic Acid-content particles (HNA) being fungal spores and pollen.  
34 We find that daily-average springtime PBAP concentration (1 to 5µm diameter) ranged between  $1.4 \times 10^4$   
35 and  $1.1 \times 10^5 \text{ m}^{-3}$ . The BioLNA population dominated PBAP during dry days ( $72 \pm 18\%$ ); HNA dominated



36 the PBAP during humid days and following rain events, where HNA (e.g., wet-ejected fungal spores)  
37 comprised up to 92% of the PBAP number. Concurrent measurements with a Wideband Integrated  
38 Bioaerosol Sensor (WIBS-4A) showed that FBAP and total FCM counts are similar; HNA (from FCM)  
39 significantly correlated with ABC type FBAP concentrations throughout the sampling period (and for the  
40 same particle size range, 1-5  $\mu\text{m}$  diameter). However, the FCM bioLNA population, possibly containing  
41 bacterial cells, did not correlate to any FBAP type. The lack of correlation of any WIBS FBAP type with  
42 the bioLNA suggest bacterial cells may be more difficult to detect with autofluorescence than previously  
43 thought. Identification of bacterial cells even in the FCM (bioLNA population) is challenging, given that  
44 the fluorescence level of stained cells at times may be comparable to that seen from abiotic particles. HNA  
45 and ABC displayed highest concentration on a humid and warm day after a rain event (4/14), suggesting  
46 that both populations correspond to wet-ejected fungal spores. Overall, information from both instruments  
47 combined reveals a highly dynamic airborne bioaerosol community over Atlanta, with a considerable  
48 presence of fungal spores during humid days, and a bioLNA population dominating bioaerosol community  
49 during dry days.

## 50 Introduction

51 Primary biological atmospheric particles (PBAP), also called bioaerosols, are comprised of airborne  
52 microbial cells (e.g. bacteria, diatoms), reproductive entities (e.g. pollen, fungal spores), viruses and  
53 biological fragments. Bioaerosols are ubiquitous, with potentially important impacts on human health,  
54 cloud formation, precipitation, and biogeochemical cycles. (Pöschl, 2005; Hoose et al., 2010; DeLeon-  
55 Rodriguez et al., 2013; Morris et al., 2014; Longo et al., 2014; Fröhlich-Nowoisky et al., 2016;  
56 Myriokefalitakis et al., 2016). Despite their low number concentration relative to abiotic particles, PBAP  
57 possess unique functional and compositional characteristics that differentiate them from abiotic aerosol.  
58 For example, certain PBAP constitute the most efficient of atmospheric ice nucleators, affecting the  
59 microphysics of mixed phase clouds and precipitation (Hoose and Möhler, 2012; Sullivan et al., 2018). The  
60 mass and nutrient content of PBAP may suffice to comprise an important supply of bioavailable P to  
61 oligotrophic marine ecosystems (Longo et al., 2014; Myriokefalitakis et al., 2016). In addition, the  
62 concurrence of disease outbreaks during dust storms has been attributed to pathogenic microbes attached  
63 to airborne dust that are subsequently inhaled (Griffin et al., 2003; Ortiz-Martinez et al., 2015; Goudie  
64 2014).

65 Quantification of the concentration and size of PBAP is critical for understanding their environmental  
66 impacts. Measuring PBAP however poses a challenge for established microbiology tools, owing to their  
67 low atmospheric concentration ( $10^3$  -  $10^6$  cells  $\text{m}^{-3}$  air; Fröhlich-Nowoisky et al., 2016) and wide diversity  
68 of airborne particle types and sizes. For instance, only a fraction of microorganisms (an estimated 5%; Chi



69 and Li et al., 2007) can be cultured, and cultivation cannot be used to quantify dead organisms, viruses or  
70 fragments, while most culture-independent methods are optimized for more abundant microbial  
71 populations. Epifluorescence microscopy (EPM) is the standard for bioaerosol quantification but is not  
72 high-throughput and requires considerable time for quantification of concentration per sample. Flow  
73 cytometry (FCM) is an analysis technique based on the concurrent measurement of light scattering and  
74 fluorescence intensity from single particles (Wang et al., 2010). FCM requires a liquid suspension of  
75 bioparticles that flows through an optical cell and interrogated with a series of laser beams. Each sample is  
76 pretreated with stains that targeting specific macromolecules (e.g. DNA/RNA) which subsequently  
77 fluoresce when excited by the FCM lasers. The resulting scattering and fluorescent light emissions are then  
78 detected by an array of sensors to allow the differentiation of biological and abiotic (e.g. dust) particles  
79 according to the characteristic specific to the stain used. FCM has proved to be as reliable as EPM, but with  
80 the advantage of lower uncertainty, higher quantification efficiency and requiring considerably less time  
81 and effort than EPM per sample (Lange et al., 1997). FCM is frequently used in biomedical research to  
82 quantify eukaryotic cell populations, and in microbiology to quantify a wide variety of yeast and bacterial  
83 cells (Nir et al., 1990; Van Dilla et al., 1983). FCM is also used to study environmental samples, e.g., to  
84 differentiate low nucleic acid (LNA) from high nucleic acid (HNA) phytoplankton in aquatic environments  
85 (Wang Y. et al 2010; Müller et al., 2010). Despite its advantages, FCM has seen little use in the bioaerosol  
86 field to date (e.g., Chen and Li, 2005; Liang et al., 2013), owing in part to the challenges associated with  
87 collecting sufficient PBAP mass for sufficient counting statistics to be obtained (Chen and Li, 2005; Liang  
88 et al., 2013). Chen and Li (2005) determined that for counting purposes, the SYTO-13 nucleic acid stain is  
89 the most effective (among five different nucleic acid stains studied) for determining reliable concentration  
90 of bioaerosols.

91 The SYTO-13 stain can also be used to provide insights on the stress/metabolic state of microbes.  
92 Guindulian et al. (1997) used FCM to study biological particles in fresh and starved seawater samples  
93 collected from the West Mediterranean Sea (Spain). Samples were analyzed either immediately or after  
94 starvation for 2-3 days. Also, *E.coli* pure cultures were tested before and after starvation in sea water. In  
95 both situations, samples were treated with DNase and RNase and subsequently stained with SYTO-13 to  
96 measure cellular DNA content (starvation ensures that intracellular RNA is negligible in marine  
97 populations, so that the SYTO-13 intensity is directly related to the DNA content of cells). Guindulian et  
98 al. (1997), with starved seawater samples and *E.coli* pure cultures together suggest that the stress level  
99 caused by marine starvation reduces RNA content in aquatic microorganisms to an undetectable level. This  
100 has important implications for the detection of atmospheric PBAP, as cells are exposed to multiple stressors  
101 when airborne.



102 Light Induced Fluorescence (LIF) is an increasingly utilized technique for bioaerosol quantification,  
103 and it relies on measuring the autofluorescence intensity of specific high yield fluorophores (e.g.,  
104 Nicotinamide Adenine Dinucleotide – NADH co-enzyme, flavins and amino acids like Tryptophan and  
105 Tyrosine) present in PBAP. The major advantage of the technique is that it is fully automated, does not  
106 require a liquid suspension (i.e., it directly senses particles suspended in air) and that provides high  
107 frequency measurements ( $\sim 1$  Hz) which make it ideal for monitoring and bioaerosol quantification.  
108 Particles detected by LIF, called Fluorescent Biological Atmospheric Particles (FBAP), although not equal  
109 to PBAP, may still constitute a large fraction of the biological particles (Healy et al., 2014; Gosselin et al.,  
110 2016). Using LIF, FBAP diurnal cycles showing maximum concentrations during evenings and minimum  
111 around middays, especially in heavily vegetated environments have been observed. This behavior has been  
112 related to known temperature and relative humidity release mechanism of certain fungal spore species (Wu  
113 et al., 2007; Gabey et al., 2010; Tropak and Schnaiter, 2013). Huffman et al. (2010) used a UV-  
114 Aerodynamic Particle Sizer (UV-APS) to show that the concentration and frequency of occurrence of  $3\mu\text{m}$   
115 FBAP particles at Mainz, Germany (semi-urban environment) exhibited a strong diurnal cycle from August  
116 through November: with a first peak at  $\sim 1.6 \times 10^4 \text{ m}^{-3}$  at mid-morning (6-8 am) followed by a constant  
117 profile ( $\sim 2\text{--}4 \times 10^4 \text{ m}^{-3}$ ) throughout the rest of the day. Similar studies in urban and densely vegetated  
118 environments suggest a notable difference in the size distributions, diurnal behavior and FBAP loading  
119 between the two environments. Gabey et al., 2011 found that the FBAP in Manchester, UK follow a  
120 characteristic bimodal distribution with peaks at  $1.2\mu\text{m}$  and  $1.5\text{--}3.0\mu\text{m}$ . As in Mainz, the concentration of  
121 larger particles peaks in the mid-morning, ranges from 0 to  $300 \text{ L}^{-1}$ , and the  $1.2\mu\text{m}$  peak is linked to traffic  
122 activity. However, at the Borneo tropical rain forest FBAP concentrations peak during the evening with a  
123 robust  $2\text{--}3\mu\text{m}$  population and concentrations ranging from 100 to  $2000 \text{ L}^{-1}$  (Gabey et al., 2010).

124 LIF-based observations (e.g. UV-APS, WIBS), combined with measurements of molecular tracers (e.g.  
125 mannitol and arabitol) and endotoxin measurements provide a more complete picture of PBAP emissions.  
126 Gosselin et al. (2016) applied this approach during the BEACHON-RoMBAS field campaign. A clear  
127 correlation between FBAP and the molecular markers is seen, indicating an increase of fungal spores during  
128 rain events. FBAP concentrations and molecular marker-inferred (arabitol and mannitol) fungal spore  
129 concentrations ( $1.7\text{pg}$  mannitol per spore and  $1.2 \text{pg}$  arabitol per spore; Bauer et al., 2008) were within the  
130 same order of magnitude. The UV-APS FBAP concentration during rain events was higher than the fungal  
131 spore concentrations inferred from the concentration of molecular markers, which suggest other non-fungal  
132 spore fluorescent particles are detected as well as fungal spores by the UV-APS. In the same study, the  
133 WIBS-3 cluster (determined using Crawford et al., 2015) linked to fungal spores gave concentrations that  
134 were 13% lower than those derived from molecular marker concentrations during rain events. During dry  
135 events, FBAP and molecular markers derived fungal spore concentrations were poorly correlated. It is



136 currently unknown the degree to which all types of PBAP are consistently detected by LIF over different  
137 time of the year and different environments; it is likely, however, that for certain classes of bioparticles  
138 (e.g., pollen and fungi) the detection efficiency using LIF is relatively high. However, the low intrinsic  
139 fluorescence intensity of bacteria and high variability of thereof in relation to metabolic state may lead to  
140 their misclassification as non-biological particles (Hernandez et al., 2016).

141 For LIF-based quantification of PBAP to be effective, it requires the intrinsic fluorescence of biological  
142 material to exceed that of non-biological matter. Depending on the type, metabolic state and species, PBAP  
143 autofluorescence may vary orders of magnitude and therefore LIF may not always be able to differentiate  
144 between biological and abiotic particles. For example, Tropak and Schnaiter (2013) showed that laboratory-  
145 generated mineral dust, soot and ammonium sulfate may be misclassified as FBAP. To address  
146 misclassification, Excitation Emission Matrices (EEMs) have been developed for biomolecules (e.g.  
147 tryptophan, tyrosine, riboflavin) and non-biological (e.g. Pyrene, Naphthalene, Humic Acid) molecules.  
148 EEMs provide the wavelength-dependent fluorescence emission spectra as a function of the excitation  
149 wavelength and are used to assign spectral modes to known fluorophores. The structure of EEMs is  
150 important for identifying molecules that are unique to PBAP and allow their identification by LIF; it is this  
151 principle upon which detectors in commercial FBAP measurements (e.g. WIBS, UV-APS) are based upon.  
152 Comparison of EEMs from biological and non-biological molecules show that even when biomolecules  
153 have higher autofluorescence intensity than non-biologicals in the LIF detection range, interferences from  
154 non-biological compounds (e.g. polycyclic aromatic hydrocarbons and soot) from combustion emissions  
155 can influence LIF detection (Pöhlker et al., 2012). Considerable work remains on determining which  
156 detector(s) or combination thereof provides an unambiguous identification of bioaerosols and related  
157 subgroups (e.g. bacteria, fungal spores, pollen). Towards this, an aerobiology catalog of pure cultures has  
158 been developed for the WIBS-4 (Hernandez et al., 2016), where, (i) pollen and fungal spore species  
159 autofluoresce much more than bacteria, and, (ii) bioaerosol subgroups are more successfully discriminated  
160 by specific detector(s). However, the same study showed that instrument-to-instrument variability in  
161 fluorescence detection poses a considerable challenge, as applying common detection thresholds across  
162 instruments leads to considerable differences in PBAP concentration and composition.

163 Another important issue for LIF-based PBAP is the impact of atmospheric oxidants, UV and other  
164 stressors on the fluorescence intensity of PBAP. This is important, given the prevalence of PBAP  
165 throughout the atmosphere, including the extreme conditions in the upper troposphere (DeLeon-Rodriguez  
166 et al., 2013). Pan et al. (2014) tested the effect of relative humidity and ozone exposure in the  
167 autofluorescence spectra of octapeptide aerosol particles using an UV-APS connected to a rotating drum.  
168 Octapeptides, organic molecules containing eight amino acids and present in cells, were used as a proxy to



169 study the aging of tryptophan and results suggest bioaerosols exposure to typical ozone concentrations  
170 (~150ppb) decrease tryptophan fluorescence intensity and affects PBAP detection. Laboratory experiments  
171 cannot always reproduce the wide variety of environmental conditions and stressors that can affect the  
172 metabolism state of microbes, and hence their autofluorescence. Joly et al. (2015) studied the survival rate  
173 of multiple bacterial (e.g. *Pseudomonas syringae*, *Sphingomonas sp.*, and *Arthrobacter sp.*) and yeast (e.g.  
174 *Dioszegia hungarica*) strains isolated from cloud water upon exposure to oxidants (e.g. H<sub>2</sub>O<sub>2</sub>), solar light  
175 (e.g. UV radiation), osmotic shocks (e.g. multiple NaCl concentrations) and freeze-thaw cycles. Among  
176 these stressors, the freeze-thaw cycles affected most the survival rate (quantified as the quotient of the  
177 colony forming unit (CFU) counts before and after exposure to each stressor dose) of bacterial cells.  
178 *Arthrobacter sp.* showed the lowest survival rates (< 20%) per cycle, and the highest survival rate of all  
179 bacterial strains was observed at 10<sup>8</sup> cell mL<sup>-1</sup> (highest concentration), suggesting that high cell  
180 concentrations lead to cell aggregation and provided protection against freeze-thaw cycles. The survival  
181 rate of the yeast *Dioszegia hungarica* was mostly affected by UV radiation showing the effect of each  
182 stressor in the survival rate of cells may depend on the characteristics of each cell. Even though the survival  
183 rate and the intrinsic fluorescence intensity of bioaerosols have not been correlated, multiple stressors can  
184 be affecting bioaerosols LIF detection and these issues regarding the use of LIF need to be resolved to fully  
185 understand their PBAP detection efficiency over the wide range of atmospheric conditions and PBAP  
186 population composition (Toprak and Schnaiter, 2013; Hernandez et al., 2016).

187 The aims of the study were to (i) develop an effective and reliable FCM detection and quantification  
188 protocol; (ii) apply the protocol to understand bioparticle populations and their variability in the metro  
189 Atlanta area during different meteorological conditions, and, (iii) compare FCM and WBS-4A results to  
190 have a better understanding of PBAP day-to-day variability. To our knowledge, this study is the first to  
191 develop a FCM protocol to identify and quantify well-defined speciated bioaerosols populations from  
192 samples collected from a modified state-of-the-art biosampler. LIF sampling of bioaerosol side-by-side  
193 with established and quantitative biology tools (FCM and EPM) was conducted to assess the LIF detection  
194 capabilities toward different bioaerosol populations and under atmospherically-relevant conditions during  
195 this study. Atlanta is selected for PBAP sampling, as it provides a highly populated urban environment  
196 surrounded by vast vegetative areas; this and the broad range of temperature and humidity ensures a wide  
197 range of PBAP population composition, state and concentrations. All the samples collected are compared  
198 side-by-side to concurrent WBS-4A data collected over the same time period.

199

200





## 201 2. Instrumentation and Methodology

### 202 2.1 Bioaerosol Sampler

203 Sampling was performed using the SpinCon II (InnovaPrep LLC, Inc.) portable wet-walled cyclone  
204 aerosol sampler. Aerosol is collected by inertial impaction with a recirculating liquid film in the cyclone;  
205 evaporative losses of the film are compensated so that the sample volume is maintained constant during a  
206 sample cycle. The particle collection efficiency for 1 $\mu$ m, 3 $\mu$ m, 3.5 $\mu$ m and 5.0 $\mu$ m particles is about  
207 47.3 $\pm$ 2.1%, 56.1 $\pm$ 3.9%, 14.6  $\pm$  0.6 and 13.8  $\pm$  2.2%, respectively (Kesavan et al., 2015). However, the  
208 experiments conducted using 1 $\mu$ m PSL and 3 $\mu$ m PSL, 3.5 $\mu$ m oleic acid and 5.0 $\mu$ m oleic acid particles not  
209 necessarily quantify the collection efficiency of biological particles in this size range. Even with a lower  
210 efficiency than any impingement sampler, SpinCon has a better performance (product of the flow rate and  
211 the sampling efficiency) than any impingement sampler due to its high volumetric flow rate, which make  
212 it more suitable for bioaerosols detection (Kesavan et al., 2015). The efficiency, power consumption and  
213 performance of 29 biosamplers were analyzed by Kesavan et al. (2015) to determine which are best suited  
214 for indoor or outdoor sampling. The study concluded biosamplers effectiveness will be determined by their  
215 performance in the size range of interest, rather than just by looking its sampling efficiency. Furthermore,  
216 Santl-Temkiv et al. (2017) recently studied SpinCon retention efficiency towards sea water heterogeneous  
217 and pure cultured *P.agglomerans* populations ( $\sim 10^5$  cells mL<sup>-1</sup>) after 1 hr sampling period by comparing  
218 FCM-derived concentrations (using SYBR green stain) before and after the sampling period. SpinCon  
219 retains 20.6 $\pm$ 5.8% of the *P.agglomerans* concentration, whereas 55.3 $\pm$ 2.1% of the sea water microbial  
220 concentration is retained after sampling for 1hr.

221 In our study, the biosampler was run at 478L min<sup>-1</sup> for 4hr sampling cycles. Phosphate-buffered saline  
222 (PBS) 1X pH 7.4 solution was used and the instrument compensated evaporation by supplying Milli-Q  
223 water to maintain the PBS concentration constant. Upon termination of each sampling cycle, the instrument  
224 was programmed to dispense the sample in a 15mL centrifuge tube. Then, 10 $\mu$ l of formalin (37 wt.%  
225 formaldehyde) per mL of solution was added to every sample for preservation and samples were stored at  
226 4°C. Given the long sampling times and the low concentration of PBAP, the fluid supply system of the  
227 instrument was modified and a cleaning protocol (CP) has been developed, which is described below.

228 SpinCon II H<sub>2</sub>O and PBS supply bags were replaced by two 2L autoclavable Nalgene bottles (Thermo  
229 Scientific Inc.) with antimicrobial tubing, connectors and a small HEPA filter connected to vent and prevent  
230 coarse and submicron particles contamination (Figure 1). Bottles were autoclaved and filled with Milli-Q  
231 water and PBS, beforehand sterilized with 0.2 $\mu$ m pore bottle top filters (Thermo Fisher Inc.) and transferred  
232 inside a biosafety cabinet. An aliquot of each fluid obtained after preparation was evaluated for sterility by  
233 EPM and FCM.



234 The cleaning protocol (CP) of the biosampling system consists of two phases. During phase one, all  
235 acrylic windows and the outside of the collector/concentrator were cleaned with ethanol 70 wt. %. Then,  
236 the instrument inlet, outlet, and the inside of the collector/concentrator was cleaned with ethanol 70 wt. %.  
237 In the second phase, the SpinCon II inlet was connected to a HEPA filter to provide a particle-free source  
238 of air to the sampling system; the instrument was then washed with ethanol 70 wt.%, 10 wt.% bleach  
239 solution, PBS and Milli-Q H<sub>2</sub>O, respectively. The wash consisted of a rinse, a 2 minutes sample and filling  
240 the instrument collector/concentrator with the fluid in use (i.e., bleach solution, ethanol, PBS and Milli-Q  
241 H<sub>2</sub>O). The collector/concentrator was drained after 1 minute. The above were repeated for the remaining  
242 fluids, taking 5 minutes per fluid. Overall, the CP requires 45 minutes; upon completion, a blank is obtained  
243 to constrain the residual contamination levels after cleaning (described below). Finally, the HEPA filter  
244 was disconnected, instrument inlets and outlets were sealed and the inlet tube was cleaned with ethanol 70  
245 wt.% to be ready for rooftop sampling. SpinCon II was rinsed with ethanol 70wt.% after each sampling  
246 episode and the cleaning protocol was applied before each sample.

247 Several blanks were obtained to quantify the levels of PBAP contamination in the fluids and sampler,  
248 and to ensure that they were sufficiently low to not bias the detection, identification and quantification of  
249 the PBAP. Furthermore, an instrument blank was obtained after a CP to constrain residual particles, by  
250 running the sampler for 2 minutes, while sampling air with a HEPA filter connected to the inlet of the  
251 SpinCon II. Another blank was collected to characterize any contamination of biological particles from the  
252 supply of PBS and water in the SpinCon II. This was done by operating the SpinCon II for a 4hr period  
253 with a HEPA filter connected to the inlet which completely cleans the air entering the wet cyclone from  
254 any bioparticles. All blanks were analyzed directly via FCM (Sect. 2.3) and EPM.

255 The volumetric flow rate within the SpinCon II was routinely calibrated by a VT100 Hotwire Thermo-  
256 anemometer (Cole Palmer Inc.) using a 3-hole round duct transverse approach. A 1 ¼" OD tube with the  
257 same diameter as the SpinCon II inlet was designed with 3 holes. Each hole was 60° apart from the other  
258 and the holes were perpendicular to the axial air flow direction of the tube. (Supplementary Information,  
259 Figure S1). Triplicates of flow rate measurements were taken in each hole at the center of the tube and  
260 averaged to determine SpinCon II volumetric flow rate ( $478.0 \pm 6.4 \text{ L min}^{-1}$ ).

## 261 2.2 Flow Cytometry

262 During this study, a BD Accuri C6 flow cytometer (BD Bioscience Inc.) was used for Flow Cytometry.  
263 The instrument quantifies suspended cells in aqueous medium at three flow velocity modes (slow, medium  
264 and fast flow at 14, 35 and 66  $\mu\text{L min}^{-1}$ , respectively). It excites particles with a 488nm laser and possesses  
265 four fluorescence detectors: FL1 ( $533 \pm 30\text{nm}$ ), FL2 ( $585 \pm 40\text{nm}$ ), FL3 ( $> 670\text{nm}$ ) and FL4 ( $675 \pm 25\text{nm}$ ),  
266 which make it possible to analyze the fluorescence from multiple dyes concurrently. In this study, 2.5  $\mu\text{M}$





267 SYTO-13 nucleic acid probe was added to the fixed samples and incubated for 15min in the dark at room  
268 temperature to stain biological particles. Additionally, 10 $\mu$ L of 15 $\mu$ m polystyrene bead suspension was  
269 added to the 1mL total volume samples as an internal standard for PBAP concentration and size  
270 quantification. The BD Accuri C6 was cleansed before each use with 0.2 $\mu$ m filtered Milli-Q water in fast  
271 mode for 10min; background particle counts were typically reduced to 1 $\mu$ L<sup>-1</sup>. At the beginning of every  
272 experiment, a 1mL blank of the atmospheric sample without SYTO-13 and beads was analyzed, used in  
273 quantification calculations (Sect. 3.1). Each sample was run in slow mode for 5min. After each sample, the  
274 instrument was flushed with 0.2 $\mu$ m filtered Milli-Q water in slow flow for 1 minute (important for robust  
275 quantification of the typically low concentrations of the atmospheric samples). SYTO-13 fluorescence  
276 intensity was quantified by the FL1-A detector and used in combination with other parameters (FSC-A &  
277 SSC-A) to constrain the PBAP populations present. FSC-A measured forward (0°  $\pm$  13°) scattering and is  
278 used to characterize the size of particles; SSC-A measured the side (90°  $\pm$  13°) scattering and is used to  
279 characterize the internal complexity (non-sphericity/shape) of particles. A 80,000 unit intensity FSC-H  
280 threshold (default FSC-H threshold value suggested by the manufacturer to minimize the effect of noise)  
281 was set in the instrument during data acquisition to minimize the effects of noise on bioparticle counts. The  
282 FSC-H channel (where H denotes height), measures single-particle forward scattering (FSC) intensity based  
283 on the peak (maximum point) of the voltage pulse curve recorded when a single particle goes through the  
284 interrogation point in the flow cytometer, whereas FSC-A, where A denotes area, measures single-particle  
285 FSC intensity based on the area below the curve of the recorder pulse. When the 80,000 unit FSC-H  
286 threshold is defined, only signals with an intensity greater than or equal to threshold value will be processed,  
287 and this could affect the statistics and detection efficiency of the flow cytometer toward small particles ( $\leq$   
288 1 $\mu$ m). Experiments conducted with 1.0 $\mu$ m polystyrene beads suspension (Supplemental information;  
289 Figure S16) have shown that 1.0 $\mu$ m beads have FSC-H intensities above the 80k threshold, no particle  
290 losses is observed, and beads estimated concentration agree with the reported by the manufacturer ( $\sim 6 \times$   
291  $10^7$  mL<sup>-1</sup>; Life Technologies, Inc.) The FCM data from each sample was analyzed using the Flow Jo  
292 software (<https://www.flowjo.com/solutions/flowjo>) to gate and quantify bioparticles population. The same  
293 procedure was used to analyze the PBS, Milli-Q water and blanks.

### 294 **2.3 LIF detection of PBAP**

295 The WIBS-4A (referred to henceforth as “WIBS”) is a single biological particle real time sensor, which  
296 measures particle light scattering and autofluorescence in an approximately 0.5 – 15 $\mu$ m particle range  
297 ([www.dropletmeasurement.com](http://www.dropletmeasurement.com)). Particles are initially sized using the 90-degree side-scattering signal  
298 from a 635 nm continuous-wave diode laser. The scattering intensity is directly related to particle diameter  
299 and was calibrated prior to deployment using polystyrene latex sphere calibration standards (PSL with 0.8,



300 0.9, 1.0, 1.3, 2.0, 3.0  $\mu\text{m}$  diameter, Thermo Scientific Inc.). The WIBS optical size therefore refers to PSL  
301 material with a real refractive index of 1.59. Healy et al. (2012) determined WIBS-4 counting efficiency by  
302 aerosolizing standardized concentrations of PSL sphere of specific sizes (e.g. 0.3, 0.4, 0.56, 0.7, 0.9 and  
303 1.3 $\mu\text{m}$ ) and compared WIBS-4 total counts against PSL counts detected by the condensation particle  
304 counter (CPC). Results show WIBS-4 possesses a 50% counting efficiency for 0.5 $\mu\text{m}$  particles and detects  
305 100% of the PSL particles above 0.7 $\mu\text{m}$  when it is compared to the CPC counts. The 280nm and 370nm  
306 pulsed Xenon flashtube UV lights in the WIBS cause the particles to autofluoresce (i.e., excite the  
307 chromophores preexisting in the PBAP and do not rely on a fluorescent dye as done in FCM). Then,  
308 fluorescent emissions are measured at three wavelength channels, which following the nomenclature of  
309 Perring et al. (2015) are: (i) channel A (“FL1\_280” in previous studies; Robinson et al., 2013), which refers  
310 to the detected emission between 310-400nm after excitation at 280nm, (ii) channel B (“FL2\_280” in  
311 previous studies), which refers to the detected emission between 420-650nm after excitation at 280nm, and,  
312 (iii) channel C (“FL2\_370” in previous studies), which refers to the detected emission between 420-650nm  
313 after excitation at 370nm. The resulting autofluorescence from 280nm excitation is affected by the presence  
314 of tryptophan, tyrosine and phenylalanine aminoacids in the PBAP (Pöhlker et al., 2012). Similarly, the  
315 resulting autofluorescence from the 370nm excitation is influenced by the presence of riboflavin and co-  
316 enzyme Nicotinamide Adenine Dinucleotide Phosphate (NAD(P)H) within the cells.

317 Biological and non-biological particles can be discriminated by using a fluorescent intensity threshold;  
318 here the threshold is determined with the Gabey et al. (2010) method and with modifications by Perring et  
319 al. (2015) as follows. Particles with fluorescence intensities below the fluorescence threshold in all channels  
320 are categorized as non-fluorescent (NON-FBAP). Particles that fluoresce above the threshold in only one  
321 channel are named with a single letter (e.g. A, B or C); particles that fluoresce in two channels are named  
322 with the two channel letters (e.g. AB, AC or BC), while particles that fluoresce in all channels are  
323 categorized as type ABC. Furthermore, the total FBAP concentration is defined as the sum of the  
324 concentration in the seven FBAP categories defined above. This approach was applied by Hernandez et al.,  
325 (2016) to pure culture PBAP (bacteria, fungal spores, pollen) to study their correspondence to FBAP types;  
326 bacteria tend to be detected by type A, and fungal spores and pollen by type AB and ABC. However,  
327 bioaerosol classification is instrument-specific and particle size dependent (Hernandez et al., 2016; Savage  
328 et al., 2017).

329 Several studies have used the Perring et al. (2015) FBAP categories to characterize PBAP in multiple  
330 environments across the globe (Yue et al., 2017; Gosselin et al. 2016 ; Yu et al., 2016). Perring et al. (2015),  
331 using a WIBS-4, studied atmospheric PBAP onboard a Skyship 600 aircraft operating between 300m and  
332 1km above ground level at 10 geographic regions across the United States; the study concluded that type



333 AB (~30%) and ABC (~25%) is the most abundant of FBAP particles in the Southeastern US (East Texas  
334 to Central Florida), and AB (~1.9  $\mu\text{m}$ ) and ABC (~2.6  $\mu\text{m}$ ) median sizes are characteristic of mold spores  
335 (fungal spores of unknown amount of species predominant on humid and warm environments;  
336 [www.cdc.gov](http://www.cdc.gov)). In addition, FBAP concentrations in the Southeastern US range from  $2 \times 10^4$  to  $8 \times 10^4 \text{ m}^{-3}$ ,  
337 constituting 3-24% of the total supermicron particle number between 1 and  $10 \mu\text{m}$  diameter. In the  
338 Southwestern US, Perring et al. (2015) shows AB and ABC types contribute less due to a higher relative  
339 contribution by types B (~25%), BC (~20%) and C (~5%), and total FBAP constitute 5-10% of the total  
340 supermicron particles. Furthermore, Perring et al. (2015) found the concentration of ABC type PBAP on  
341 the surface and aloft did not vary throughout the Southeastern US. In the highly vegetated Rocky Mountains  
342 Gosselin et al. (2016) found (using a WIBS-3) that ABC type particles always are a significant fraction of  
343 FBAP (at least 20%) and are especially enhanced during rainy days (during or post-rain events) to ~ 65%  
344 of the total FBAP, owing to the release of wet-ejected fungal spores following precipitation (Huffman et  
345 al., 2013). However, during dry days, types BC and C increase their relative fraction to ~30% and ~40%,  
346 respectively (Perring et al., 2015). Limited studies have looked closely at the FBAP categories in urban  
347 environments. In Nanjing, China, Yu et al. (2016) observed that types B (~45%), BC (~25%) and C (~15%)  
348 dominate the FBAP concentrations during autumn. All FBAP types, except type C, correlated with black  
349 carbon and  $\text{PM}_{0.8}$  concentrations (particle mass with diameter below  $0.8 \mu\text{m}$ ), suggesting a strong  
350 interference by combustion sources; Type C PBAP ( $6.6 \times 10^5 \pm 5.5 \times 10^5 \text{ m}^{-3}$ ) was considered more  
351 representative of bioaerosols, although with unknown interference from abiotic particles. Similarly, Yue et  
352 al. (2017) found a dominance of type B PBAP (~66% of total FBAP) during clean and polluted events in  
353 wintertime Beijing, China; interestingly, the FBAP contribution to the total particle concentration is higher  
354 during polluted events (13-24%) than during clean events (12-14%). FL1 type particles (sum of types AC,  
355 ABC, AB and A) are more abundant in clean periods (~25%) than in polluted periods (10.1%), while the  
356 fraction of type C FBAP is higher during polluted periods (~20%) than during clean periods (~5%).

#### 357 **2.4 Location of sampling site and sampling frequency**

358 Bioaerosol sampling was conducted between April 7 and May 15, 2015 at the rooftop sampling  
359 platform of the Ford Environmental Sciences and Technology (ES&T) building at the Georgia Institute of  
360 Technology campus in Atlanta, GA. The site, which was located at the heart of a major urban environment,  
361 is surrounded by dense forested areas in the southeastern USA: the Oconee National Forest (South East),  
362 the Chattahoochee National Forest (North), and the Talladega National Forest (West). The WIBS was  
363 operating continuously throughout the same period, sampling bioaerosol from a 15 ft. long and  $\frac{1}{4}$  in. ID  
364 conductive tubing inlet fixed 8 ft. above the sampling platform floor. The SpinCon II was placed in the  
365 platform during sampling episodes with its inlet facing South. Three 4-hour samples per week were  
366 collected with the Spincon II sampler over the 5-week period (4 h sampling between 10am and 5pm; Table



367 1). Meteorological data acquired from the same platform provided wind speed, wind direction, relative  
368 humidity (RH), temperature, total hourly rain and UV radiation index with a 1min resolution.

369

### 370 **3. Data processing and Analysis**

#### 371 **3.1 FCM data processing**

372 All blanks collected showed contamination levels that did not exceed 1% of the PBAP quantified in the  
373 subsequent atmospheric samples. The 2-minute instrument blanks obtained after the CP and the HEPA filter  
374 washes was  $1.06 \times 10^3 \pm 7.37 \times 10^2 \text{ mL}^{-1}$  and  $9.22 \times 10^2 \pm 1.24 \times 10^2 \text{ mL}^{-1}$ , respectively, which are negligible  
375 accumulations compared to the  $2.55 \times 10^5 \pm 1.14 \times 10^5 \text{ mL}^{-1}$  average PBAP concentration quantified in the  
376 atmospheric samples. The concentration of PBAP in the blanks was also confirmed with microscopy (not  
377 shown). Based on this, we are confident that the CP protocol and procedure to replace the working fluids  
378 ensured sterility of the biosampler before each sampling.

379 FCM analysis of the samples was carried out as follows. We obtain the fluorescence intensity (from  
380 each of the 4 fluorescence detectors), forward scattering and side scattering intensity for all the particles  
381 suspended in the samples. A gating procedure was used to determine the fluorescence levels associated  
382 with detecting only particles containing SYTO-13 (hence, a PBAP) and background fluorescence from non-  
383 stained particles. The procedure (Supplemental information, SI.2 and SI.3) consists of 3 steps: (a)  
384 fluorescence threshold determination, (b) population gating, and, (c) biological/non-biological particle  
385 discrimination in the population(s) within the threshold (e.g. LNA PBAP, Section 4.1). The fluorescence  
386 threshold was determined using an atmospheric sample without SYTO-13 collected before each FCM  
387 analysis, as a blank. Based on the fluorescence responses obtained, we determine the FL1-A fluorescence  
388 intensity value for which 99.5% or 99.9% of the (unstained) particles of the blank autofluoresce below the  
389 chosen value. This FL1-A intensity, called “fluorescence threshold”, was determined for each sample  
390 (supplementary information, Figure S2a and S2b). The determination of the fluorescence threshold  
391 involved selecting the most conservative value that maximizes inclusion of biological particles and  
392 minimizes the inclusion of non-biological particles, including those that may be subject to background  
393 fluorescence or unspecific binding of SYTO-13 (Diaz et al., 2009; Müller et al., 2010). We found out that  
394 threshold values for the 99.9% approach were substantially higher than 99.5% approach in multiple  
395 sampling events and comparable to the fluorescence intensities observed for stained pure cultures ( $\sim 10^5$   
396 units), which means that the 99.9% threshold values will miscount pure cultures as non-biological.  
397 Consequently, we set the fluorescence threshold to the highest fluorescence intensity value observed by the  
398 99.5% approach (41,839 units; supplementary information, Figure S2b), applied it to all collected samples;  
399 henceforth named the 42k FL1-A threshold. The 42k threshold value aims to minimize any abiotic



400 interference as it maximizes biological particles quantification. A fixed value has been chosen and applied  
401 to all samples given that having a different threshold value for each sampling event may result in  
402 quantification biases as bioaerosols with strong autofluorescence (e.g. pollen, fungal spores) can increase  
403 the threshold value and affect PBAP quantification in the population(s) within the threshold. The BD Accuri  
404 C6 flow cytometer used for the analysis of the samples maintains constant pre-optimized photomultiplier  
405 voltages and amplifier gain settings. As a result, the fluorescence intensity of particles is consistent from  
406 day-to-day, and the fluorescence intensity of a specific biological particle population having the same  
407 metabolic state and physiological characteristics must not show day-to-day variability  
408 (www.bdbiosciences.com). Under the 42k threshold approach PBAP concentrations in the population(s)  
409 within the threshold (e.g. LNA, Section 4.1) can be overestimated by up to a 0.5%. Furthermore, FCM  
410 experiments conducted with unprocessed Arizona Test Dust (ATD) show that the FL1\_A intensity  
411 distribution of SYTO-13 stained ATD particles is very similar to unstained ATD particles, and 100% of the  
412 SYTO-13 stained ATD particles stay below the 42k threshold (supplemental information, Figure S14a and  
413 S14b), supporting the 42k threshold effectiveness to filter out abiotic particles.

414 Once the FL1-A threshold was determined, plots of FL1-A vs. SSC-A and FL1-A vs. FSC-A are used  
415 to define clusters of bioparticles with fluorescence that exceed the FL1-A threshold and a characteristic  
416 optical size (obtained from the FSC-A intensity) or particle shape/complexity (obtained from the SSC-A  
417 intensity). FL1-A vs. SSC-A plots were used to define the populations of bioparticles for PBAP  
418 quantification as clusters using SSC-A parameter were more defined and showed better spatial resolution  
419 than using FSC-A parameter. The limits of each population were also determined with Flow Jo  
420 (www.flowjo.com), using 2% contour plots (supplemental information; Figure S3) generated by equal  
421 probability contouring (i.e., 50 contour levels so that the same number of cells fall between each pair of  
422 contour lines). Populations above the FL1-A threshold value (41,839 FL1-A units) were considered  
423 biological (Section 4.1; e.g. HNA); the particles in the population within the threshold value (Section 4.1;  
424 e.g. LNA) having a FL1-A intensity greater than 41,839 units were counted as biological to determine the  
425 PBAP counts in the population. The total PBAP counts were considered as all particles counts having FL1-  
426 A fluorescence intensity above the determined threshold value minus the 15µm beads internal standard  
427 having FL1-A fluorescence intensity above the determined threshold value. The 15µm beads of known  
428 concentration and particle size allows for calibrating the optical size (supporting information, SI.7) of the  
429 bioparticles, as well as their concentration and departure from sphericity. The 15µm beads population  
430 showed fluorescence intensities comparable to the determined fluorescence threshold after been stained  
431 with SYTO-13 as it is known that molecular stains can be adsorbed on the surface of polystyrene beads  
432 (Eckenrode et al., 2005; Rödiger et al., 2011). The relatively high fluorescence intensity of the 15µm beads  
433 show populations within the threshold value (e.g. LNA, Section 4.1) cannot be rule out as being affected



434 by unspecific staining of abiotic particles. However, populations above the threshold value (e.g. HNA,  
435 Section 4.1) should not be affected by such abiotic interferences.

### 436 3.2 WIBS data processing

437 15-minute average total aerosol and FBAP size distributions were obtained from the WIBS. FBAP was  
438 distinguished from the total aerosol using the Gabey et al. (2010) “trigger threshold” approach, which is  
439 applied as follows. First, the average “electronic fluorescence noise” and its standard deviation is  
440 determined for each channel (A, B, C) performing the Force Trigger (FT) calibration which consist to  
441 operate the WIBS without flowing air through the system. The FT calibration, carried out every 24hr, is  
442 critical for determining the lowest particle autofluorescence levels that robustly exceeds instrument  
443 electronic noise. FT calibrations measured the particle-free air background autofluorescence in the three  
444 WIBS channels (e.g. A, B, C), and measurements recorded the fluorescence intensity for 500 excitation  
445 flash events (Ziemba et al., 2016; Tropak and Schnaiter, 2013; Gabey et al., 2010). The threshold for each  
446 detector is then equal to the average fluorescence plus 2.5 times its standard deviation; particles with  
447 fluorescence intensities above this threshold value are classified as FBAP. Then, Perring et al. (2015)  
448 approach (Section 2.3) is applied to determine the combination of thresholds that provide the maximum  
449 concentration of PBAP and minimal interference from abiotic particles, which still remains an area of active  
450 research. WIBS-3 and WIBS-4 models have been actively studied to determine which channel best detect  
451 bioaerosols and to cluster different types of PBAP (Robinson et al., 2013; Crawford et al., 2014; Gabey et  
452 al., 2010). Both models use filtered xenon flash lamps to excite particles at 280nm and 370nm wavelengths  
453 and detect PBAP autofluorescence in two regimes (For WIBS-3, FL1: 320-600nm and FL2: 410-600nm;  
454 For WIBS4, FL1: 310-400nm and FL2; 420-650nm). Three separate fluorescence channels for each model:  
455 (i) channel A: detection in FL1 following 280nm excitation, (ii) channel B: detection in FL2 following  
456 280nm excitation and (iii) channel C: detection in FL2 following 370 nm excitation, are then available for  
457 FBAP determination. The main difference between WIBS models is that the fluorescence detection regimes  
458 overlap in channels A and B for the WIBS-3, but not for the WIBS-4. WIBS-3 FBAP quantification cannot  
459 be compared directly with WIBS-4 due to channel A and B overlap, but FBAP detection in all channels  
460 have been consistent between both models (Robinson et al., 2013). WIBS-4 contains two switchable gain  
461 settings (e.g. high gain (HG), low gain (LG)), allowing it to measure 0.5µm to 12µm particles in HG and  
462 3µm to 31µm particles in LG setting. On the other hand, the second generation of the WIBS-4, named  
463 WIBS-4A, maintains single gain settings and evaluates particles between 0.5µm and 20µm (Fennelly et al.,  
464 2017).

465 Gabey et al. (2011) concluded, using a WIBS-3, that channel C was most efficient in quantifying FBAP  
466 either in the Borneo tropical forest or in the urban environment of Manchester, UK. Healy et al. (2014)  
467 found higher channel A FBAP concentration in Killarney, Ireland using WIBS-4. Pure culture experiments





468 with WIBS-4 have shown high detection efficiency of channel A toward *Pseudomonas syringae* bacteria  
469 (Tropak et al., 2013). Hernandez et al. (2016) used WIBS-4 to test the intrinsic fluorescence fingerprints of  
470 29 fungi, 13 pollen and 15 bacteria species and suggested channel A is most suitable for discriminating  
471 bacteria and fungi, channel C is most suitable for pollen and channel B can be influenced by abiotic  
472 particles. In addition, among FBAP categories (Perring et al., 2015) bacteria is mainly detected as type A,  
473 fungal spores shown multiple fluorescence types (e.g. A, AB, BC and ABC) and pollen is mainly detected  
474 as type BC and ABC. However, PBAP detection effectiveness by specific channels varies considerably  
475 between instruments, which suggests a thorough calibration may be necessary. Furthermore, Savage et al.  
476 (2017) used WIBS-4A to show FBAP fluorescence also varies with particle size, especially for pollen and  
477 fungal spores and proposed pathways of change by which particles may transition from type A or type B to  
478 type ABC as they increase size. FBAP type variation with particle size is important to consider as the  
479 approach of Perring et al. (2015) is used to better understand what FBAP type is best detected (e.g. bacteria,  
480 fungal spores, pollen).

481 In this study, thresholds for each channel were determined daily, and the total particle concentration,  
482 FBAP types (e.g. A, B, C, AB, BC, AC, ABC) concentrations and the total FBAP concentration (sum of  
483 the seven FBAP types) were used. From the data, 4h-averaged size distributions (using 15-minute average  
484 data) were generated for the total particles and all FBAP types in the 1-10 $\mu$ m range during the time SpinCon  
485 II run. Subsequently, WIBS overall sampling efficiency (aspiration efficiency + transport efficiency) was  
486 calculated using the Particle Losses Calculator (Von der Weiden et al., 2009) and applied to the 1-10 $\mu$ m  
487 size distributions for the sampling characteristics in our setup (15ft. sampling line with 1/4 in. ID and 2.3 L  
488 min<sup>-1</sup> flow rate; Figure S4a). The sampling efficiency was calculated to be 67% for 5 $\mu$ m particles, with  
489 larger losses as size increased to 10 $\mu$ m. (supplemental information, FigureS4b). FCM and WIBS total  
490 particles and PBAP comparison was constrained to the 1 to 5 $\mu$ m range being the size overlap of both  
491 techniques. Also, the fractional composition of FBAP (based on number concentrations) was calculated to  
492 characterize its daily variability (Section 4.2), and compared against the daily variability of PBAP from the  
493 FCM analysis (Section 4.4).

## 494 **4. Results and Discussion**

### 495 **4.1 FCM biopopulation identification and quantification**

496 When the FCM results are plotted in terms of FL1-A intensity versus SSC-A intensity, four populations  
497 (Figure 2) emerge above the threshold gating process: low nucleic acid (LNA) particles, high nucleic acid  
498 (HNA) particles, pollen and the 15 $\mu$ m internal standard beads. EPM and SEM pictures (Supplementary  
499 Figures S5, S6, and S7) confirm the presence of these heterogeneous populations. Previously, LNA and  
500 HNA populations were identified in FCM of aquatic samples with the use of the SYTO-13, SYBR green



501 and DAPI nucleic acid stains (Wang Y. et al 2010; Bouvier, T. et al 2007; Lebaron, P. et al 2001);  
502 corresponding populations in atmospheric PBAP have not been identified before. Below we focus on each  
503 population to further identify them as pollen, fungal spores, bacteria and other fragments.

504 The HNA size distributions are dominated by 3-5 $\mu\text{m}$  particles (mean diameter:  $4.15 \pm 0.06 \mu\text{m}$ ;  
505 Supplemental Information, Figure S10) and the total concentration strongly correlated with RH. HNA were  
506 virtually non-existent during extended dry periods (days with average RH < 70% during sampling, e.g. 4/9,  
507 4/22 and 5/15) and well defined during periods of high humidity, especially after rain events (days with  
508 average RH > 70% and T > 18 °C during sampling episode; e.g. 4/7, 4/14, 4/15). Both these characteristics  
509 suggest that HNA particles correspond to fungal spores (e.g., from the Ascospores and Basidiospores genus;  
510 Oliveira et al., 2000; Li and Kendrick, 1995). The LNA size distributions are dominated by 2-4  $\mu\text{m}$  particles  
511 (mean diameter:  $2.99 \pm 0.06\mu\text{m}$ ; Supplemental Information, Table S1) and dominated Atlanta PBAP  
512 composition during dry days. The LNA population shows SYTO-13 fluorescence intensities that are about  
513 one order of magnitude lower than the HNA population. The observed particle sizes are within the size  
514 range of airborne bacteria (Després et al., 2012) and the LNA population may represent single or  
515 agglomerated bacterial cells. However, it is clear that heterogeneous populations will probably contain  
516 multiple types of microorganisms and that may be the case in the LNA population.

517 It is known that pollen may burst into tiny fragments when is suspended in water (e.g., Augustin et al.,  
518 2012; Taylor et al., 2007). Therefore, pollen may fragment during sampling and processing of samples in  
519 the FCM, increasing the concentration of LNA particles and biasing concentrations. FCM applied to  
520 ragweed pollen suggests a 1:2 pollen-to-pollen fragments concentration ratio (Supplementary information,  
521 Table S2). Also, calculations based upon FCM-derived ragweed pollen and pollen fragments concentrations  
522 during this study (considering the total pollen mass added to the sample, 15 $\mu\text{m}$  mean diameter previously  
523 determined by Lin et al. (2013) and unit density) suggest approximately 67% of the ragweed pollen grains  
524 were intact after hydration and that each fragmented grain generates ~5 pollen fragments; in agreement  
525 with Bacsi et al. (2006), 35% of ragweed pollen fragments upon hydration. Overall, ragweed pollen results  
526 suggest FCM experiments do not have a considerable impact in pollen fragmentation and that pollen  
527 fragmentation will have a negligible effect on LNA concentrations. Ragweed pollen is one of the most  
528 abundant wind-driven pollen species in the United States and its emission peaks during fall, but can be also  
529 present during late spring and summer. It is representative of the pollen species we see in the Atlanta area  
530 (Darrow et al., 2012) and results suggest pollen fragmentation would not generate a substantial amount of  
531 fragments. The low collection efficiency of SpinCon toward large particles (<14% for diameters above  
532 5 $\mu\text{m}$ ) and that pollen concentrations in our samples are generally two orders of magnitude lower than LNA  
533 concentrations suggest a negligible effect of pollen fragments in LNA biological particle quantification.



534 Also, EPM results showed intact pollen and limited amounts of small debris among the particles identified  
535 in the atmospheric samples collected for this study. Particles with fluorescence intensities above the FL1-  
536 A threshold value were counted as biological, giving us the PBAP counts within the LNA population and  
537 will be referred henceforth as the “bioLNA” population (Figure 2).

538 A population of strongly fluorescing and very large particles (10-20 $\mu\text{m}$ , avg. average geometric mean  
539 diameter  $12.3 \pm 1.7\mu\text{m}$ ) was identified (Figure 2). This population also strongly autofluoresces in the FCM  
540 when SYTO-13 was not added to the sample (SI.7, Figure S11). All together this indicates a population of  
541 pollen particles, as they are known to contain cell wall compounds (i.e., phenolic compounds, carotenoid  
542 pigments, Phenylcoumarin) that fluoresce more strongly than the proteins and cytosolic compounds  
543 responsible for bacteria/fungi autofluorescence (Pöhlker et al., 2012; Hill et al., 2009; Pöhlker et al., 2013).  
544 The pollen population was not well-defined during all sampling events; whenever present, pollen was  
545 characterized by concentrations ( $\sim 10^2 \text{ m}^{-3}$ ) consistent with reported values (Despres et al., 2012), which are  
546 also much lower than bioLNA and HNA concentrations. As a result, pollen population was systematically  
547 gated using a perfect square between  $10^6$  and  $10^8$  intensity units in the FL1-A vs. SSC-A plot for each  
548 atmospheric sample. bioLNA, HNA and pollen counts, acquired by the 42k threshold approach were used  
549 to calculate liquid-based ( $\text{mL}^{-1}$  of sample solution) and air-based ( $\text{m}^{-3}$  of air) concentrations for each  
550 bioaerosol population as detailed in the Supplemental Information. The total PBAP concentration on each  
551 sample consisted of all non-bead particles above the 42k fluorescence threshold given that a non-negligible  
552 biological particle concentration was not constrained in the gated populations. Even though the 2% contour  
553 plots effectively allowed population gating,  $16.5 \pm 7.3\%$  of the total PBAP are not attributed the identified  
554 populations. The biological particles not constrained by gating, henceforth named as the “unclassified”  
555 bioparticles, showed the highest concentrations when both HNA and LNA populations are densely  
556 populated (4/16, 4/28 and 5/14; Figure 5). The lowest concentrations were observed when just the LNA  
557 population is identified (4/9, 4/22, 5/15; Figure 5) and when the LNA and HNA populations are identified  
558 after the rain event on 4/14. The observed behavior shows that the unclassified bioparticle concentrations  
559 is linked to the heterogeneity of the biological populations and the concentration of the gated populations  
560 (e.g. HNA, LNA and Pollen). The “unclassified” bioparticles concentration ranges from  $8.1 \times 10^2 \text{ m}^{-3}$  to  
561  $1.3 \times 10^4 \text{ m}^{-3}$  (avg.  $4.2 \times 10^3 \pm 3.3 \times 10^3$ ) and they are not constrained to a specific size range. In addition,  
562 we must note that additional concentration corrections are required owing to the sampling efficiency of the  
563 SpinCon II, but will be considered in sections 4.3 and 4.4.

564 Before SpinCon II sampling efficiency corrections are applied, FCM total particle concentrations range  
565 from  $2.6 \times 10^4 \text{ m}^{-3}$  to  $2.9 \times 10^5 \text{ m}^{-3}$ , with increasing concentrations toward the end of the sampling period.  
566 In addition, total PBAP concentration averaged  $2.4 \times 10^4 \pm 1.1 \times 10^4 \text{ m}^{-3}$  (coefficient of variation, CV, 13%;  
567 defined as the standard deviation over a triplicate FCM measurements over the average concentration).



568 BioLNA ranged between  $6.8 \times 10^2$  and  $2.9 \times 10^4 \text{ m}^{-3}$  (average:  $1.1 \times 10^4 \text{ m}^{-3}$ ; CV: 20%), HNA (fungal spores)  
569 between  $4.7 \times 10^3$  and  $1.9 \times 10^4 \text{ m}^{-3}$  (average:  $1.1 \times 10^4 \text{ m}^{-3}$ ; CV: 15%) when above the detection limit ( $n=12$ ),  
570 and pollen from  $1.3 \times 10^2$  to  $1.2 \times 10^3 \text{ m}^{-3}$  (average:  $3.6 \times 10^2 \text{ m}^{-3}$ ; CV: 21%). These concentration levels are  
571 consistent with microscopy-based studies in urban environments for bacteria (e.g.,  $1.7 \times 10^4 \pm 1.3 \times 10^4 \text{ m}^{-3}$   
572 in springtime Birmingham, UK; (Harrison et al., 2005); fungal spores ( $1.8 \times 10^4 \pm 1.1 \times 10^4 \text{ m}^{-3}$  in Vienna,  
573 Austria between April-June; Bauer et al., 2008); and pollen (between  $5.69 \times 10^2 \text{ m}^{-3}$  to  $6.144 \times 10^3 \text{ m}^{-3}$  in  
574 Medellin, Colombia; Guarín et al., 2015). Also, additional experiments performed in September 2015,  
575 described in Figure S7 of the supplemental information (supplemental information, SI.6), showed that EPM  
576 and FCM-based quantifications agree within an order of magnitude. This is consistent with Lange et al.  
577 (1997), whom also found that FCM gives higher quantifications than EPM microscopy when studying *P.*  
578 *aeruginosa* pure cultures and airborne bacteria collected from a swine confinement building in Iowa, USA.

579 To better understand SYTO-13 fluorescence intensity differences between the identified (e.g. bioLNA,  
580 HNA and pollen) populations in the atmospheric samples and their metabolic/stress state, FCM experiments  
581 were conducted with air-isolated bacteria (F8 strain; De Leon Rodriguez, 2015), ragweed pollen and yeast  
582 (*S. cerevisiae*; Y55 strain) mixtures to compare the SYTO-13 fluorescence intensity and the scattering  
583 properties of the pure cultures to those seen in the atmospheric samples. Pure cultures and atmospheric  
584 samples are summarized in Tables S3, S4 (supplementary information; FCM pure culture experiments)  
585 respectively. The bioLNA population showed SYTO-13 fluorescence intensity up two orders of magnitude  
586 lower than F8 bacteria. HNA (fungal spores) population showed an order of magnitude lower SYTO-13  
587 fluorescence intensity than Y55 HNA yeast, and, within the same magnitude for the LNA Y55 yeast. The  
588 HNA and LNA yeast populations in the pure culture experiments (Figure S13a) have one order of  
589 magnitude difference in FL1-A fluorescence intensity and may represent yeast populations with different  
590 metabolic states. Atmospheric and Ragweed pollen populations had similar SYTO-13 fluorescence  
591 intensities and Figure S13c shows pollen fluorescence intensity may go up to  $10^8$ . The lower SYTO-13  
592 fluorescence intensity of the atmospheric populations may be related to genetic material degradation from  
593 exposure to atmospheric stressors; depending on the physiological characteristics of each population (Zhen  
594 et al., 2013; Amato et al., 2015). Our results also agree with Guindulian et al. (1997), showing that *E.coli*  
595 overnight cultures have higher SYTO-13 fluorescence intensity than starved *E.coli* population. Overall,  
596 FCM pure culture results suggest microbes starve in the atmosphere, leading to a possible reduction or  
597 leakage of the amount genetic material enclosed within each cell. Sampling can also stress cells, even  
598 disrupt the wall/membrane of the cell and lead to genetic material leakage (Zhen et al., 2013).

599 Pollen, HNA (fungal spores) and bioLNA atmospheric populations showed different SYTO-13  
600 fluorescence intensities. Pollen showed the highest fluorescence intensity, followed by the HNA and



601 bioLNA (fraction of LNA above threshold; Figure 2) populations, respectively (Figure 2; Table S4).  
602 Guindulian et al. (1997) FCM results with starved bacterioplankton from seawater samples treated with  
603 DNase/RNase showed SYTO-13 fluorescence intensity can be related to the DNA content of starved  
604 bacterioplankton due to the low amount of RNA enclosed in starved cells. Taking in consideration our  
605 results and previous studies, we can suggest that Pollen, bioLNA and HNA populations in the atmospheric  
606 samples are differenced by their DNA content, which can in part explain SYTO-13 fluorescence intensity  
607 difference between them. Future work is needs to further study this.

608

#### 609 **4.2 WIBS total concentration and FBAP daily variability**

610 WIBS-4A collected data continuously throughout the period; for comparison against the SpinCon  
611 II 4h liquid batch samples, WIBS data was averaged to the SpinCon II sampling times (Table 1). WIBS  
612 total particle concentration (1-5 $\mu$ m diameter) ranged from  $2.0 \times 10^5$  to  $1.0 \times 10^6$  m<sup>-3</sup> in agreement with  
613 observed particle concentrations in previously studied urban environments during Spring/Summer months  
614 like Helsinki, Finland (UV-APS avg.  $1.6 \times 10^5$  m<sup>-3</sup>; Saari et al., 2015) and Karlsruhe, Germany (WIBS-4  
615 avg.  $6.9 \times 10^5$  m<sup>-3</sup>; Tropak and Schnaiter et al., 2013). 4h average total particles concentrations in Figure 3a  
616 show particle concentrations declined during rain episodes (during or post-rain: e.g. 4/15, 4/16, 4/28, 4/29,  
617 4/30) as wet removal of PBAP is most efficient. However, during dry (no rain) episodes total particle  
618 concentrations built up in the atmosphere. To better understand the day-to-day variability of different FBAP  
619 types, the seven Perring et al. (2015) FBAP categories (e.g. Type A, B, C, AB, AC, BC and ABC) were  
620 studied plus the NON-FBAP type constituting particles that do not fluoresce in any channel (e.g. channel  
621 A, B, C). NON-FBAP concentrations are one order of magnitude higher than FBAP concentrations, and  
622 NON-FBAP, hence traced WIBS total particles throughout all sampling events (Figure 3a). Total FBAP  
623 concentrations also show similar behavior to the total particle concentration (Figure 3a) and it suggests non-  
624 biological particles can be biasing the total FBAP concentration. The variability of the total FBAP  
625 concentration is mainly linked to type A and type B concentrations as overall they constitute the two largest  
626 fractions to the total FBAP concentration (Figure 3b), and both FBAP types have previously misidentified  
627 non-biological particles as FBAP (Tropak and Schnaiter et al., 2013; Yu et al., 2016). As a result, our study  
628 considers the total FBAP concentration as the upper limit, and ABC type concentration as the lower limit  
629 of FBAP concentration in Metro, Atlanta. Type B dominates the FBAP fractional composition (Figure 3b),  
630 which has been linked to possible non-biological interferences from black carbon (Yu et al., 2016) and  
631 polycyclic aromatic hydrocarbons (PAHs) emitted from combustion sources. Total FBAP fraction ranges  
632 from 16% and 43%, and ABC fraction ranges from 1.3% and 9.2% of the total particles in the 1 to 5 $\mu$ m  
633 size range. ABC type fractions and ABC type concentrations are within the values observed by Tropak and



634 Schnaiter (2013) using WIBS-4 in Karlsruhe, Germany; averaging  $2.9 \times 10^4 \text{ m}^{-3}$  (when considering the sum  
635 of AC and ABC types) and constituting 7% of total coarse mode particles ( $0.8\mu\text{m}$ - $16\mu\text{m}$ ).

636 ABC type concentrations show an interesting variability throughout the 15 sampling events, as  
637 ABC reaches its maximum concentration on 4/14, on a warm and humid day after a rain event, concurrently  
638 when the FCM HNA population also reaches its highest concentration – strongly suggesting ABC particles  
639 are fungal spores. (Figure 3a, Table 1). Recently, Gosselin et al. (2016) used WIBS-3 in the Rocky  
640 Mountains, Colorado showing ABC type fractional composition enhances after rain events to dominate the  
641 total FBAP composition and the enhancement is correlated to mannitol and arabitol concentrations (fungal  
642 spore tracers), which have been previously linked to Ascomycota and Basidiomycota spores emitted by the  
643 wet-ejection mechanism (Elbert et al., 2007). In addition, ABC type constitute a considerable fraction  
644 (~20%) of total FBAP during dry days in the Rocky Mountains possible because such highly vegetative  
645 environments maintain a high background of fungal spores (Huffman et al., 2013). However, urban  
646 environments like Metro Atlanta are not necessary dominated by fungal spores and its FBAP composition  
647 will be affected by the biological sources close to city (e.g. forests), local emissions and meteorology. The  
648 overall FBAP composition in metro Atlanta (Figure 3b) is dominated by type B (avg. fraction:  $33 \pm 9\%$ ),  
649 type A (avg. fraction:  $22 \pm 5\%$ ) and type AB (avg. fraction:  $22 \pm 5\%$ ) particles. Type ABC constitute  $12 \pm$   
650  $6\%$  of the total FBAP and it reaches 30% on 4/14, comparable to values observed by Gosselin et al., 2016  
651 in the Rocky Mountains. The dominance of type B particles has been observed in the polluted atmosphere  
652 of Nanjing, China using WIBS-4A were type B constituted ~ 45% of the total PBAP and type B ( $\sim 2 \times 10^6$   
653  $\text{m}^{-3}$ ) concentrations were up to two orders of magnitude higher than type A concentrations ( $\sim 5 \times 10^4 \text{ m}^{-3}$ )  
654 suggesting a high likelihood of interference from abiotic particle sources. However, Metro-Atlanta shows  
655 much lower total particle concentrations than Nanjing, China ( $\sim 10^7 \text{ m}^{-3}$ ) and type A and type B  
656 concentrations are within the same order of magnitude. Furthermore, Perring et al. (2015) have shown type  
657 B particles constitute a considerable fraction of the total supermicron particles across the United States,  
658 being ~15% and ~25% over (altitude >100m) the Southeastern US and Southwestern US, respectively.  
659 Total particle and NON-FBAP size distributions in Figure 3c peaked at  $\sim 1\mu\text{m}$ . Similarly, types A, B, AB  
660 size distributions (Figure 3d) peaked close to  $1\mu\text{m}$  showing that interferences by non-biological particles  
661 cannot be rule out. However, ABC type size distribution (red line, Figure 3d) is dominated by 3- $5\mu\text{m}$   
662 particles and ABC type particles may have come from a different source to other FBAP types as they get  
663 enhanced after rain events (e.g. 4/14; Table 1). Yu et al. (2016) also observed 4- $6\mu\text{m}$  ABC type particles  
664 in the highly polluted Nanjing, China, but ABC type bimodal size distributions showed a peak between 1-  
665  $2\mu\text{m}$  and a second peak between 4- $6\mu\text{m}$ . In addition, ABC type number fractions in Nanjing, China  
666 correlated to black carbon mass fractions suggesting a considerable influence by combustion related





667 particles and no rain events occurred during the sampling period. The difference between Metro Atlanta  
668 and Nanjing, China ABC type size distributions suggest ABC type is not influenced by combustion related  
669 particles in Metro Atlanta. Overall, results show FBAP concentration (1-5 $\mu\text{m}$ ) ranges from  $10^4$  -  $10^5$   $\text{m}^{-3}$  in  
670 metro Atlanta and wet-ejected fungal spores concentration, detected by ABC type, can constitute up to 30%  
671 of the FBAP (1-5  $\mu\text{m}$ ) after rain events.

#### 672 **4.3 Correlation of HNA population with ABC type**

673 A quantitative comparison between WBS-4A total particle and FCM total particle concentrations  
674 was subsequently performed and we focused the analysis to the 1 to 5 $\mu\text{m}$  size range as SpinCon sampling  
675 efficiency is reduced significantly above 5 $\mu\text{m}$  ( $\leq 14\%$ ; Kesavan et al., 2015). WBS-4A and FCM total  
676 particle concentrations differed by about one order of magnitude (for optical diameter,  $d_o$ , greater than  
677 1.5 $\mu\text{m}$ ) and particle concentration difference increased for particles with  $d_o < 1.5$   $\mu\text{m}$  as shown in the size  
678 distribution (geometrically averaged across the 15 SpinCon II sampling events) in Figure 4a. The largest  
679 difference between WBS-4A and uncorrected FCM size distributions seems to be related to SpinCon II  
680 having a cutoff size close to 1 $\mu\text{m}$ , reducing significantly its sampling efficiency. Even with the observed  
681 difference in the magnitude of the concentrations between the two techniques, ABC type and HNA  
682 concentrations traced throughout all the sampling events and are highly correlated ( $R^2 = 0.40$ ; Figure 4b)  
683 and showed similar size distributions in the 1 to 5 $\mu\text{m}$  range as shown in Figure S12a. HNA and ABC type  
684 were both dominated by 3-5 $\mu\text{m}$  particles and it seems both are detecting the same type of biological  
685 particles. In addition, AB type showed a weak correlation with HNA concentrations ( $R^2 = 0.17$ ), but their  
686 size distributions differed as type AB peaks close to  $\sim 1\mu\text{m}$  (Figure 3d). ABC is the only FBAP type showing  
687 a considerable correlation to the HNA population, and bioLNA population is not correlated with any FBAP  
688 type. Overall, ABC type and HNA correlation is an important step forward to better understand the  
689 effectiveness of WBS-4A FBAP categories to provide speciated PBAP concentrations in urban areas. ABC  
690 type particles have shown substantial concentrations ( $10^4$ - $10^5$   $\text{m}^{-3}$ ; Perring et al., 2015; Ziemba et al., 2016)  
691 across the US. The highest ABC fraction of the total FBAP was observed in Panhandle, Florida during an  
692 airborne study among multiple environments studied using WBS-4A to sample from the California coast  
693 to central Florida, suggesting ABC type particles are ubiquitous in the US (Perring et al., 2015). Previous  
694 studies (Healy et al., 2014, Huffman et al., 2013) have shown correlations between LIF technology (e.g.  
695 WBS-4 and UV-APS) fluorescence channels and fungal spores number concentrations, especially during  
696 fungal spores invigoration after rain events. Healy et al. (2014) used WBS-4 in Killarney National Park,  
697 Ireland (e.g. high vegetative rural area) finding correlations between channel B (FL2;  $R^2 = 0.29$ ) and channel  
698 C (FL3;  $R^2 = 0.38$ ) concentrations and fungal spores concentrations (collected by Sporewatch impactor and  
699 quantified by microscopy). However, now for the first time FCM HNA population have shown a correlation  
700 with WBS-4A ABC type and suggests ABC type category detects well actively ejected fungal spores in



701 Metro Atlanta (e.g. urban area). In addition, recent WIBS-4A experiments using pure cultures have shown  
702 ABC type detects well several fungal spores (e.g. *Aspergillus Versicolor* & *Botrytis* spp.) and small pollen  
703 grains, but detection may vary across instruments (Hernandez et al., 2016).

704 FCM concentrations were corrected based on correction factors (CF) calculated upon the  
705 comparison of ABC and HNA size distributions (1 to 5 $\mu$ m) for each sampling event given (1) ABC type  
706 and HNA population similar size distributions and number concentrations (1 to 5 $\mu$ m) correlation, and, (2)  
707 WIBS-4A provides us representative concentrations of airborne particle concentrations in Metro Atlanta  
708 after sampling losses being corrected (Section 3.2). Concentration correction factors were determined for  
709 each sampling episode by taking the quotient of ABC type to HNA concentrations over the 1-5 $\mu$ m size  
710 range. The resulting size-dependent correction factor (Figure S12b) was then applied to the FCM size  
711 distributions, giving the “corrected FCM” bioaerosol data (between 1 and 5  $\mu$ m). Figure 4a shows that the  
712 corrected FCM total particle average size distribution traces WIBS-4A size distribution, allowing us to  
713 correct for SpinCon II low collection efficiency and to better constrain the magnitude of FCM  
714 concentrations. Our approach to calculate the estimated collection efficiency (ECE) considers all the  
715 processes that affect the concentration of PBAP, from collection to final quantification in the FCM. Figure  
716 S12b compares Kesavan et al. (2015) collection efficiencies determined for SpinCon I and the estimated  
717 collection efficiency calculated upon the CF calculation ( $ECE = 1/CF$ ) and shows the ECE of the SpinCon  
718 II is lower than Kesavan et al. (2015) below 3 $\mu$ m and performs better for particles above 3 $\mu$ m, but above  
719 3 $\mu$ m Kesavan et al (2015) collection efficiency is within the uncertainty of our calculations. Our lower ECE  
720 values (Figure S12b) for particles below 3 $\mu$ m can be related to SpinCon sampling time as Kesavan et al.  
721 (2015) experiment were conducted in a short period of time (e.g. 10-15 min) and ours took place for 4 hr.  
722 The main mechanisms leading to below 3 $\mu$ m particle losses could be their re-aerosolization over time being  
723 lost through the blower exhaust of the SpinCon II (Figure 1). Also, coagulation of small particles over time  
724 can not be ruled out, but future work is needed to study it.

725

#### 726 **4.4 PBAP populations after collection/detection corrections**

727 After correction through the application of the ABC correction factors, FCM total particle  
728 concentrations (1 to 5 $\mu$ m avg.:  $5.5 \times 10^5 \pm 5.1 \times 10^5$  m<sup>-3</sup>; Figure 5a) are within the same order of magnitude  
729 as WIBS-4A concentrations (1 to 5 $\mu$ m avg.:  $5.4 \times 10^5 \pm 2.9 \times 10^5$  m<sup>-3</sup>; Figure 3a), and continue to exhibit  
730 substantial variability. The HNA (e.g. fungal spores) population showed a substantial invigoration during  
731 three sampling events (4/7, 4/14, 4/15; Figure 5a and 5b). To better understand the role of meteorology on  
732 PBAP composition, the PBAP samples were classified into four regimes based on the average diurnal  
733 relative humidity and ambient temperature, with  $T = 18$  °C (65 °F) to differentiate between warm and cold



734 days, and, RH = 70% to differentiate between humid and dry days. The temperature and RH threshold  
735 values were chosen based on the observations and understanding that a combination of temperature and RH  
736 within these threshold values can significantly impact bioaerosol composition. For instance, humid and  
737 warm conditions may lead to the invigoration of fungal spores by wet ejection from plants (Ingold, 1971),  
738 on contrary, PBAP will get stressed when exposed to warm and dry conditions. The sampling times, RH,  
739 ambient temperature and meteorological categories of each SpinCon II sample is presented in Table 1.

740 Humid and warm days (4/7, 4/14 and 4/15; light green shaded areas in Figure 5a) were characterized  
741 by well-defined HNA and bioLNA populations. These sampling episodes had the highest average HNA  
742 (fungal spore) concentration ( $4.0 \times 10^4 \pm 1.3 \times 10^4 \text{ m}^{-3}$ ) among the four meteorological regimes and during  
743 these sampling events HNA constituted  $\geq 77\%$  of the total PBAP. Among the humid and warm days (Figure  
744 5a and 5b), average bioLNA, HNA and “unclassified” bioaerosol compositions were 6.1%, 84.0% and  
745 9.9%, respectively of the total PBAP number. Also, the humid and warm days occurred after rain events,  
746 which can be linked directly to the strong fungal spore invigoration (Huffman et al., 2013). Before sampling,  
747 early morning precipitation occurred during 4/14 and 4/15, as well as during the night of 4/6. Precipitation  
748 did not occur during sampling in any of the humid and warm days. The FCM results (Figure S15a-c) that  
749 display the PBAP population between 4/7 and 4/9 show a disappearance of the (HNA) fungal spore  
750 population during the transition from a “humid and warm” day (4/7) to a “dry and warm” day (4/9). Figure  
751 5b shows how the HNA contribution to the total PBAP goes down on 4/8 when RH decreases and is  
752 undetected on 4/9. Furthermore, Figure 6a-c shows FL1 vs. SSC-A plots for 4/14 to 4/16 consecutive  
753 sampling periods, where a marked increase in the bioLNA concentration from 4/15 to 4/16 goes together  
754 with a striking decrease in the HNA concentration. HNA fraction went down from 92.05% to 34.1% of the  
755 total PBAP and bioLNA concentration went up from  $3.8 \times 10^3 \text{ m}^{-3}$  to  $2.9 \times 10^4 \text{ m}^{-3}$ . Humid and Warm days  
756 had the lowest averaged PBAP concentration ( $4.6 \times 10^4 \pm 9.8 \times 10^3 \text{ m}^{-3}$  in the 1 to  $5 \mu\text{m}$  range) among the  
757 four meteorological regimes, a possible effect of the bioaerosols being lost by wet scavenging, resulting in  
758 the enhancement of fungal spore contribution to the total PBAP number concentrations. The unclassified  
759 biological particles concentration also showed its lowest contribution ( $2.9 \times 10^3 \text{ m}^{-3}$ ; 9.9%) to the total  
760 PBAP number concentration during these events, when the HNA and LNA populations are best identified  
761 by the 2% contour plots.

762 Cold and humid days (4/16 and 4/29; light yellow shaded areas in Figure 5a) also showed well-defined  
763 HNA population, and HNA contributed on average to  $29.5 \pm 6.5\%$  of the total PBAP concentration (1 to  
764  $5 \mu\text{m}$ ). On 4/16 drizzling took place by the end of the sampling period, but no accumulated rainfall was  
765 measured by the meteorological station. However, on 4/29, accumulated rainfall averaged 0.04in. from  
766 11:55 AM to 2:20 PM (Figure S21). The similar HNA concentration between “Humid and Warm” and



767 “Humid and Cold” days seen in Figure 5a and the lower contribution of HNA to the total PBAP during the  
768 “Humid and Cold” days may be linked to previously suggested bacteria emissions by droplet soil impaction  
769 during rain events (Joung et al., 2017). Bacteria emission by soil impaction can increase airborne bioLNA  
770 concentration and HNA (fungal spores) will have a lower contribution to the total PBAP even when the  
771 fungal spore concentration is high during rain events. Both cold and humid days showed a considerable  
772 difference in bioLNA contributions to the total PBAP concentration. On 4/16 and 4/29 bioLNA constituted  
773 45.2% and 65.3% of the total PBAP concentration, respectively (Figure 5b). The difference in the bioLNA  
774 contribution to the total PBAP can be linked to the intensity of precipitation, as it shapes the composition  
775 (e.g. size and types) of microbes suspended in the atmosphere during the different stages of a rainfall (e.g.  
776 before, on set, during and after a rainfall; Yue et al., 2016).

777 Six of the fifteen sampling days were classified as warm and dry (4/8, 4/9, 4/22, 5/13, 5/14, 5/15; light  
778 orange shaded areas in Figure 5a) and it did not rain before or during any of these days (Table 1). During  
779 warm and dry days, HNA had the lowest averaged concentration ( $8.7 \times 10^3 \pm 1.2 \times 10^4 \text{ m}^{-3}$ ) among the four  
780 meteorological categories. In addition, during three dry and warm days (4/9, 4/22 and 5/15) the HNA  
781 population was undetected. This behavior can be related to the fact that high RH drives fungal spore  
782 emissions by wet ejection, but soil wetness could also affect emissions because the HNA population was  
783 detected in other warm and dry days with comparable RH (Huffman et al., 2013; Gosselin et al., 2016). The  
784 air mass trajectories reaching Atlanta during each sampling event could also affect the biological particles  
785 composition. For example, on 4/22, when the HNA was undetected, the 500m and 100m 72 h backward air  
786 mass trajectories reaching Atlanta came from the NW (US/Canada border) at high altitudes and do not  
787 spend more than 24h near surface. This air mass could affect bioaerosol composition with minimal  
788 influence from local bioaerosol emissions. However, the enhancement or the depletion of the HNA  
789 population have not been linked to specific air masses trajectories. Besides meteorology, two main  
790 hypotheses could explain the observed behavior in the HNA population, previously stated by Bouvier et  
791 al., 2007 to understand HNA and LNA populations in aquatic environments, but also applicable to airborne  
792 microorganisms. First, microbes might begin in the HNA population upon aerosolization and then move to  
793 the LNA upon death or inactivity. Second, the HNA and LNA populations may contain completely different  
794 microbial taxa and have different organisms in each population. If the first hypothesis occurs, we expect to  
795 see a covariance of the HNA and LNA FCM parameters (e.g. FSC-A, SSC-A and FL1-A intensities), and  
796 observe a gradual decrease in the FL1-A intensity of the HNA population to the FL1-A values observed by  
797 particles in the LNA population, which is not seen. Although our results suggest the HNA and LNA are  
798 two distinctive populations, further studies will have to take place to sort and directly study the DNA  
799 sequences of each population in order to prove the second hypothesis. HNA population behavior may also  
800 consist of a combination of both hypotheses. Overall, warm and dry days prevail during springtime in



801 Atlanta and bioLNA contribution (avg.:  $3.4 \times 10^4 \pm 2.5 \times 10^4 \text{ m}^{-3}$ ) may represent the bioaerosol background  
802 of Atlanta.

803 Four of the fifteen sampling days (4/21, 4/23, 4/28 and 4/30; light blue shaded areas in Figure 5a) were  
804 characterized by cold and dry conditions (Table 1). PBAP were dominated by bioLNA during these events,  
805 as can see in Figure 7a-c, where LNA population are the dominant contributors to PBAP number. HNA  
806 population was diminished in Figure 7a (4/21) & Figure 7c (4/23) during cold and dry days and disappeared  
807 in Figure 7b during a warm and dry day. Overall, HNA was detected during cold and dry days, but showed  
808 lower contributions to the total PBAP number concentration than humid days. Among cold and dry days,  
809 the PBAP population (1 to 5  $\mu\text{m}$ ) was composed on average of  $72.6 \pm 10.1\%$  bioLNA and  $16.5 \pm 8.2\%$   
810 HNA. Cold and dry days had on average the highest bioLNA ( $5.3 \times 10^4 \pm 1.8 \times 10^4 \text{ m}^{-3}$ ) and total PBAP  
811 ( $7.3 \times 10^4 \pm 2.0 \times 10^4 \text{ m}^{-3}$ ) number concentrations (1 to 5 $\mu\text{m}$ ) among the four meteorological categories,  
812 reaching the PBAP maximum concentration on 4/23 (Figure 5a).

813

#### 814 **4.5 PBAP day-to-day variability in Metro Atlanta: FCM vs. WIBS**

815 Although WIBS and FCM possess different methodologies, they show similar trends providing a  
816 good understanding of the daily variability of PBAP in Metro Atlanta. FCM PBAP fraction (1 to 5 $\mu\text{m}$ )  
817 ranges from 3.8% to 69.2% of the total particles and the highest PBAP fraction (69.2%) and HNA  
818 concentration is observed on 4/14 ( $5.25 \times 10^4 \pm 5.89 \times 10^3 \text{ m}^{-3}$ ). The total FBAP fraction (1 to 5 $\mu\text{m}$ ) ranges  
819 from 16% to 43%, but it reaches its maximum on 4/15. However, ABC fraction of the total WIBS particle  
820 concentration ranges from 1.3% to 9.2% and it reaches its maximum on 4/14. Even when the magnitudes  
821 of the PBAP and FBAP fractions differ on average by a factor of  $\sim 2$  throughout the sampling period, both  
822 techniques agree an enhancement in the total biological particles takes place between 4/14 to 4/16. Given  
823 the uncertainty of the two methodologies, it is remarkable that there is such agreement between WIBS and  
824 FCM results.

825 Among the four meteorological categories, humid and warm days characterize for showing the  
826 highest HNA, A type, AB type and ABC type concentrations suggesting that A and AB types may also be  
827 related to wet-ejected fungal spores in Metro Atlanta; this possibly explains why the ABC fraction of the  
828 total FBAP in 4/7 is not as high as on 4/14 and 4/15 (Figure 3b), and differs with the behavior observed by  
829 the HNA population on 4/7. The bioLNA population does not show a correlation to any specific FBAP type  
830 and shows its highest concentrations during dry and cold days. In addition, bioLNA concentrations are  
831 anticorrelated with type B concentrations (Figure S19, correlation coefficient,  $r = -0.59$ ;  $R^2 = 0.30$ ) during  
832 dry (both cold and warm) days, when bioLNA dominates the total PBAP concentration. Given that type B  
833 particles have been previously correlated to abiotic particles (e.g. black carbon) in urban environments (Yue



834 et al., 2017), bioLNA and type B anticorrelation suggests that bioLNA particles may in fact represent a  
835 heterogeneous bioaerosol population. That bioLNA is not correlated with any FBAP type gives rise to two  
836 possibilities: (1) if bioLNA population is mainly composed of bacteria or agglomerated bacteria, then it is  
837 possible that they are detected by multiple FBAP types and is not attributed specifically to one of them; (2)  
838 the intrinsic fluorescence of bioLNA particles is too low and a high fraction of them is abiotic. It is  
839 challenging to determine what PBAP types each WIBS FBAP type is mainly detecting. Based on WIBS-  
840 4A results in Metro Atlanta, ABC type detects wet-ejected fungal spores, but still unclear what PBAP types  
841 are detected by the other FBAP types or if they just capture a high fraction of non-biological particles. FBAP  
842 types and WIBS total particles correlations in Figure S17 show all FBAP types are correlated to WIBS total  
843 particles, but ABC and AB types show the lowest correlations (type AB:  $R^2 = 0.101$ ; type ABC:  $R^2 =$   
844  $0.1266$ ).

845 Figure 8 shows FCM total PBAP (black line), ABC type (light green), FL1 (Channel A; dark green  
846 line) and total FBAP (blue line) concentrations, where the FL1 concentration ( $[FL1]$ ) constitutes the sum  
847 of the number concentrations of types A, AB, AC, and ABC ( $[FL1] = [A] + [AB] + [AC] + [ABC]$ ; Gabey  
848 et al., 2011; Healy et al., 2014). Throughout the April-May 2015 sampling events, total PBAP  
849 concentrations (1 to  $5\mu\text{m}$ ) were mainly constrained between the FL1 and ABC type concentrations  
850 suggesting FL1 and ABC type represent the upper and lower bound PBAP concentrations in Metro Atlanta,  
851 respectively. It is also important to highlight that FCM PBAP concentrations are closer to the ABC type  
852 concentrations before April 16 when the HNA population dominates, but then after April 16 FCM PBAP  
853 concentrations are closer to FL1 concentrations when bioLNA starts to dominate the total PBAP  
854 concentration. In addition, Figure 8 shows that total FBAP (sum of type A, B, C, AB, AC, ABC) exceeds  
855 the (corrected) PBAP concentrations in Metro Atlanta.

856

## 857 5. Conclusions

858 In this study we presented the development and testing of an effective FCM protocol to identify and  
859 quantify bioaerosol populations. The FCM protocol, designed to constrain any particle accumulation due  
860 to cleaning or by fluid supplies, successfully quantified the day-to-day variability of bioaerosols in the  
861 Atlanta Metro area. It is the first FCM study to detect well-defined LNA (low nucleic acid) and HNA (high  
862 nucleic acid) atmospheric biological populations under different meteorological scenarios. FCM results  
863 show dynamic bioaerosol populations in Atlanta leading to a 84.0% of HNA (wet-ejected fungal spores)  
864 and 6.1% bioLNA contribution to the PBAP number (1 to  $5\mu\text{m}$  range), respectively, during humid and  
865 warm days after rain events. However, bioLNA dominates warm and cold dry days, constituting 72% of  
866 the PBAP number concentration.





867 WIBS-4A and SpinCon II collocated sampling showed that the HNA and ABC type concentrations are  
868 well correlated ( $R^2=0.40$ ) and display similar size distribution. We therefore conclude that both instruments  
869 detect the same particles, and used empirical collection/detection efficiency factors to correct the FCM size  
870 distributions and concentrations in the 1 to 5 $\mu\text{m}$  diameter range. WIBS-4A and FCM results suggest Metro  
871 Atlanta PBAP concentrations range between  $10^4 - 10^5 \text{ m}^{-3}$  (1 to 5 $\mu\text{m}$ ) and they can constitute a substantial  
872 fraction of coarse mode particle concentration (WIBS-4A: 43%; FCM: 69%), comparable to the PBAP  
873 coarse mode fraction in highly vegetated environments. The FCM bioLNA population, possibly containing  
874 bacterial cells, did not correlate to any FBAP type. The fact that the bioLNA population is not correlated  
875 with a specific FBAP type suggests it may be particularly challenging to use LIF techniques to distinguish  
876 bioaerosols with low intrinsic autofluorescence from non-biological particles, especially given the  
877 heterogeneities introduced by the large biodiversity of airborne microbes. The possible influence of abiotic  
878 particles in the bioLNA population can also explain the lack of correlation between bioLNA and FBAP  
879 types given that the FCM threshold approach does not ensure total exclusion of abiotic particles. In addition,  
880 the unspecific binding of SYTO-13 to abiotic particles cannot be ruled out in the bioLNA population. FCM  
881 comparison between atmospheric and pure culture samples showed lower SYTO-13 fluorescence  
882 intensities in the atmospheric samples and suggests a degradation in the genetic material of PBAP, possibly  
883 caused by the limited nutrients and strong stress prevailing in the atmosphere, which further challenge the  
884 ability of LIF to distinguish bioLNA.

885 In summary, this study have shown for the first time that FCM can effectively identify, quantify and  
886 study the daily variability of heterogeneous PBAP populations (e.g. HNA, bioLNA and pollen) with  
887 different genetic material content in an urban environment to the degree of quantitatively correlate FCM  
888 HNA to WIBS-4A ABC type number concentrations and better understand wet-ejected fungal spores  
889 enhancement after rain events. Furthermore, FCM and WIBS-4A results show bacterial cells detection and  
890 quantification still a challenging task for LIF technology as well as for FCM given the complexity involved  
891 to minimize abiotic interferences, and to the heterogenicity of the atmospheric samples.

892

### 893 **Acknowledgments**

894 We acknowledge support from a Georgia Power Faculty Scholar chair, a Cullen-Peck Faculty Fellowship,  
895 a Dreyfus Foundation Postdoctoral Fellowship in Environmental Chemistry, NASA, and a NASA Earth  
896 System Science Fellowship. We also thank Prof. Rodney Weber for helpful suggestions on the SpinCon II  
897 flow calibration.

898



## 899 References

- 900 Amato, P., Joly, M., Schaupp, C., Attard, E., Möhler, O., Morris, C. E., Brunet, Y., and Delort, A. M.:  
901 Survival and ice nucleation activity of bacteria as aerosols in a cloud simulation chamber, *Atmospheric*  
902 *Chemistry and Physics Discussions*, 15, 4055-4082, [10.5194/acpd-15-4055-2015](https://doi.org/10.5194/acpd-15-4055-2015), 2015.
- 903 Atkinson, R. W., Strachan, D. P., Anderson, H. R., Hajat, S., and Emberlin, J.: Temporal associations  
904 between daily counts of fungal spores and asthma exacerbations, *Occup Environ Med*, 63, 580-590,  
905 [10.1136/oem.2005.024448](https://doi.org/10.1136/oem.2005.024448), 2006.
- 906 Augustin, S., Hartmann, S., Pummer, B., Grothe, H., Niedermeier, D., Clauss, T., Voigtländer, J.,  
907 Tomsche, L., Wex, H., and Stratmann, F.: Immersion freezing of birch pollen washing water,  
908 *Atmospheric Chemistry and Physics Discussions*, 12, 32911-32943, [10.5194/acpd-12-32911-2012](https://doi.org/10.5194/acpd-12-32911-2012), 2012.
- 909 Bacsi, A., Choudhury, B. K., Dharajiya, N., Sur, S., and Boldogh, I.: Subpollen particles: carriers of  
910 allergenic proteins and oxidases, *J Allergy Clin Immunol*, 118, 844-850, [10.1016/j.jaci.2006.07.006](https://doi.org/10.1016/j.jaci.2006.07.006),  
911 2006.
- 912 Bauer, H., Claeys, M., Vermeylen, R., Schueller, E., Weinke, G., Berger, A., and Puxbaum, H.: Arabitol  
913 and mannitol as tracers for the quantification of airborne fungal spores, *Atmospheric Environment*, 42,  
914 588-593, [10.1016/j.atmosenv.2007.10.013](https://doi.org/10.1016/j.atmosenv.2007.10.013), 2008.
- 915 Bauer, H., Schueller, E., Weinke, G., Berger, A., Hitzengerger, R., Marr, I. L., and Puxbaum, H.:  
916 Significant contributions of fungal spores to the organic carbon and to the aerosol mass balance of the  
917 urban atmospheric aerosol, *Atmospheric Environment*, 42, 5542-5549, [10.1016/j.atmosenv.2008.03.019](https://doi.org/10.1016/j.atmosenv.2008.03.019),  
918 2008.
- 919 Bouvier, T., Del Giorgio, P. A., and Gasol, J. M.: A comparative study of the cytometric characteristics of  
920 high and low nucleic-acid bacterioplankton cells from different aquatic ecosystems, *Environ Microbiol*, 9,  
921 2050-2066, [10.1111/j.1462-2920.2007.01321.x](https://doi.org/10.1111/j.1462-2920.2007.01321.x), 2007.
- 922 Bowers, R. M., McLetchie, S., Knight, R., and Fierer, N.: Spatial variability in airborne bacterial  
923 communities across land-use types and their relationship to the bacterial communities of potential source  
924 environments, *ISME J*, 5, 601-612, [10.1038/ismej.2010.167](https://doi.org/10.1038/ismej.2010.167), 2011.
- 925 Chen, P. S., and Li, C. S.: Bioaerosol characterization by flow cytometry with fluorochrome, *J Environ*  
926 *Monit*, 7, 950-959, [10.1039/b505224f](https://doi.org/10.1039/b505224f), 2005.
- 927 Chi, M.-C., and Li, C.-S.: Fluorochrome in Monitoring Atmospheric Bioaerosols and Correlations with  
928 Meteorological Factors and Air Pollutants, *Aerosol Science and Technology*, 41, 672-678,  
929 [10.1080/02786820701383181](https://doi.org/10.1080/02786820701383181), 2007.
- 930 Crawford, I., Robinson, N. H., Flynn, M. J., Foot, V. E., Gallagher, M. W., Huffman, J. A., Stanley, W.  
931 R., and Kaye, P. H.: Characterization of bioaerosol emissions from a Colorado pine forest: results from  
932 the BEACHON-RoMBAS experiment, *Atmospheric Chemistry and Physics Discussions*, 14, 2499-2552,  
933 [10.5194/acpd-14-2499-2014](https://doi.org/10.5194/acpd-14-2499-2014), 2014.
- 934 Darrow, L. A., Hess, J., Rogers, C. A., Tolbert, P. E., Klein, M., and Sarnat, S. E.: Ambient pollen  
935 concentrations and emergency department visits for asthma and wheeze, *Journal of Allergy and Clinical*  
936 *Immunology*, 130, 630-638.e634, <https://doi.org/10.1016/j.jaci.2012.06.020>, 2012.



- 937 DeLeon-Rodriguez, N., Terry L. Lathem, Luis M. Rodriguez-R, James M. Barazesh, Bruce E. Anderson,  
938 Andreas J. Beyersdorf, Luke D. Ziemba, Michael Bergin, Athanasios Nenes, and Konstantinos T.  
939 Konstantinidis.: Microbiome of the upper troposphere: Species composition and prevalence, effects of  
940 tropical storms, and atmospheric implications, *Proceedings of the National Academy of Sciences* 110,  
941 2575-2580, 2013.
- 942 DeLeon-Rodriguez, N.: Microbes in the atmosphere: prevalence, species composition, and relevance to  
943 cloud formation School of Biology Georgia Institute of Technology, 129 pp.,  
944 (<http://hdl.handle.net/1853/55517>), 2015.
- 945 Després, V. R., Alex Huffman, J., Burrows, S. M., Hoose, C., Safatov, A. S., Buryak, G., Fröhlich-  
946 Nowoisky, J., Elbert, W., Andreae, M. O., Pöschl, U., and Jaenicke, R.: Primary biological aerosol  
947 particles in the atmosphere: a review, *Tellus B*, 64, 10.3402/tellusb.v64i0.15598, 2012.
- 948 Díaz, M., Herrero, M., García, L. A., and Quirós, C.: Application of flow cytometry to industrial  
949 microbial bioprocesses, *Biochemical Engineering Journal*, 48, 385-407,  
950 <https://doi.org/10.1016/j.bej.2009.07.013>, 2010.
- 951 Eckenrode, H. M., Jen, S.-H., Han, J., Yeh, A.-G., and Dai, H.-L.: Adsorption of a Cationic Dye Molecule  
952 on Polystyrene Microspheres in Colloids: Effect of Surface Charge and Composition Probed by Second  
953 Harmonic Generation, *The Journal of Physical Chemistry B*, 109, 4646-4653, 10.1021/jp045610q, 2005.
- 954 Elbert, W., Taylor, P. E., Andreae, M. O., & Pöschl, U.: Contribution of fungi to primary biogenic  
955 aerosols in the atmosphere: wet and dry discharged spores, carbohydrates, and inorganic ions.,  
956 *Atmospheric Chemistry and Physics*, 7, 4569-4588, 2007.
- 957 Fennelly, J. M., Sewell, G., Prentice, B. M., O'Connor, J. D., and Sodeau, R. J.: Review: The Use of  
958 Real-Time Fluorescence Instrumentation to Monitor Ambient Primary Biological Aerosol Particles  
959 (PBAP), *Atmosphere*, 9, 10.3390/atmos9010001, 2018.
- 960 Fröhlich-Nowoisky, J., Kampf, C. J., Weber, B., Huffman, J. A., Pöhlker, C., Andreae, M. O., Lang-  
961 Yona, N., Burrows, S. M., Gunthe, S. S., Elbert, W., Su, H., Hoor, P., Thines, E., Hoffmann, T., Després,  
962 V. R., and Pöschl, U.: Bioaerosols in the Earth system: Climate, health, and ecosystem interactions,  
963 *Atmospheric Research*, 182, 346-376, <http://dx.doi.org/10.1016/j.atmosres.2016.07.018>, 2016.
- 964 Gabey, A. M., Gallagher, M. W., Whitehead, J., Dorsey, J. R., Kaye, P. H., and Stanley, W. R.:  
965 Measurements and comparison of primary biological aerosol above and below a tropical forest canopy  
966 using a dual channel fluorescence spectrometer, *Atmospheric Chemistry and Physics*, 10, 4453-4466,  
967 10.5194/acp-10-4453-2010, 2010.
- 968 Gabey, A. M., Stanley, W. R., Gallagher, M. W., and Kaye, P. H.: The fluorescence properties of aerosol  
969 larger than 0.8  $\mu\text{m}$  in urban and tropical rainforest locations, *Atmospheric Chemistry and Physics*, 11,  
970 5491-5504, 10.5194/acp-11-5491-2011, 2011.
- 971 Gosselin, M. I., Rathnayake, C. M., Crawford, I., Pöhlker, C., Fröhlich-Nowoisky, J., Schmer, B.,  
972 Després, V. R., Engling, G., Gallagher, M., Stone, E., Pöschl, U., and Huffman, J. A.: Fluorescent  
973 bioaerosol particle, molecular tracer, and fungal spore concentrations during dry and rainy periods in a  
974 semi-arid forest, *Atmos. Chem. Phys.*, 16, 15165-15184, 10.5194/acp-16-15165-2016, 2016.
- 975 Goudie, A. S.: Desert dust and human health disorders, *Environment International*, 63, 101-113,  
976 <http://dx.doi.org/10.1016/j.envint.2013.10.011>, 2014.



- 977 Griffin, D. W., Kellogg, C. A., Garrison, V. H., Lisle, J. T., Borden, T. C., and Shinn, E. A.: Atmospheric  
978 microbiology in the northern Caribbean during African dust events, *Aerobiologia*, 19, 143-157,  
979 10.1023/B:AERO.0000006530.32845.8d, 2003.
- 980 Guarín, F. A., Abril, M. A. Q., Alvarez, A., and Fonnegra, R.: Atmospheric pollen and spore content in  
981 the urban area of the city of Medellin, Colombia, *Hoehnea*, 42, 9-19, 2015.
- 982 Guindulain, T., J. Comas, and J. Vives-Rego: Use of nucleic acid dyes SYTO-13, TOTO-1, and YOYO-1  
983 in the study of *Escherichia coli* and marine prokaryotic populations by flow cytometry, *Applied and*  
984 *environmental microbiology*, 63, 4608 - 4611, 1997.
- 985 Harrison, R. M., Jones, A. M., Biggins, P. D. E., Pomeroy, N., Cox, C. S., Kidd, S. P., Hobman, J. L.,  
986 Brown, N. L., and Beswick, A.: Climate factors influencing bacterial count in background air samples,  
987 *International Journal of Biometeorology*, 49, 167-178, 10.1007/s00484-004-0225-3, 2005.
- 988 Healy, D. A., Huffman, J. A., O'Connor, D. J., Pöhlker, C., Pöschl, U., and Sodeau, J. R.: Ambient  
989 measurements of biological aerosol particles near Killarney, Ireland: a comparison between real-time  
990 fluorescence and microscopy techniques, *Atmos. Chem. Phys.*, 14, 8055-8069, 10.5194/acp-14-8055-  
991 2014, 2014.
- 992 Healy, D. A., O'Connor, D. J., and Sodeau, J. R.: Measurement of the particle counting efficiency of the  
993 "Waveband Integrated Bioaerosol Sensor" model number 4 (WIBS-4), *Journal of Aerosol Science*, 47,  
994 94-99, <http://dx.doi.org/10.1016/j.jaerosci.2012.01.003>, 2012.
- 995 Hill, S. C., Mayo, M. W., and Chang, R. K.: Fluorescence of bacteria, pollens, and naturally occurring  
996 airborne particles: excitation/emission spectra, Army Research Lab Adelphi Md Computational And  
997 Information Sciences Directorate, 2009.
- 998 Hoose, C., Kristjánsson, J. E., and Burrows, S. M.: How important is biological ice nucleation in clouds  
999 on a global scale?, *Environmental Research Letters*, 5, 024009, 2010.
- 1000 Hoose, C., and Möhler, O.: Heterogeneous ice nucleation on atmospheric aerosols: a review of results  
1001 from laboratory experiments, *Atmos. Chem. Phys.*, 12, 9817-9854, 10.5194/acp-12-9817-2012, 2012.
- 1002 Huffman, J. A., B. Treutlein, and U. Pöschl: Fluorescent biological aerosol particle concentrations and  
1003 size distributions measured with an Ultraviolet Aerodynamic Particle Sizer (UV-APS) in Central Europe,  
1004 *Atmospheric Chemistry and Physics*, 10, 3215-3233, 2010.
- 1005 Huffman, J. A., Prenni, A. J., DeMott, P. J., Pöhlker, C., Mason, R. H., Robinson, N. H., Fröhlich-  
1006 Nowoisky, J., Tobo, Y., Després, V. R., Garcia, E., Gochis, D. J., Harris, E., Müller-Germann, I., Ruzene,  
1007 C., Schmer, B., Sinha, B., Day, D. A., Andreae, M. O., Jimenez, J. L., Gallagher, M., Kreidenweis, S. M.,  
1008 Bertram, A. K., and Pöschl, U.: High concentrations of biological aerosol particles and ice nuclei during  
1009 and after rain, *Atmospheric Chemistry and Physics*, 13, 6151-6164, 10.5194/acp-13-6151-2013, 2013.
- 1010 Ingold, C. T.: *Fungal spores. Their liberation and dispersal*, Oxford, Clarendon Press., 302 pp. pp., 1971.
- 1011 Jung, Y. S., and Buie, C. R.: Aerosol generation by raindrop impact on soil, 6, 6083,  
1012 10.1038/ncomms7083, <https://www.nature.com/articles/ncomms7083#supplementary-information>, 2015.
- 1013 Kesavan, J., and Sagripanti, J. L.: Evaluation criteria for bioaerosol samplers, *Environ Sci Process*  
1014 *Impacts*, 17, 638-645, 10.1039/c4em00510d, 2015.



- 1015 Lange, J. L. T., P S and Lynch, N: Application of flow cytometry and fluorescent in situ hybridization for  
1016 assessment of exposures to airborne bacteria Appl. Environ. Microbiol. , 63, 1557-1563, 1997.
- 1017 Lebaron, P., Servais, P., Agogue, H., Courties, C., and Joux, F.: Does the high nucleic acid content of  
1018 individual bacterial cells allow us to discriminate between active cells and inactive cells in aquatic  
1019 systems?, Appl Environ Microbiol, 67, 1775-1782, 10.1128/AEM.67.4.1775-1782.2001, 2001.
- 1020 Li, D.-W., and Bryce Kendrick: A year-round study on functional relationships of airborne fungi with  
1021 meteorological factors, International Journal of Biometeorology 39, 74-80, 1995.
- 1022 Liang, L., Engling, G., Cheng, Y., Duan, F., Du, Z., and He, K.: Rapid detection and quantification of  
1023 fungal spores in the urban atmosphere by flow cytometry, Journal of Aerosol Science, 66, 179-186,  
1024 10.1016/j.jaerosci.2013.08.013, 2013.
- 1025 Lin, H., Gomez, I., and Meredith, J. C.: Pollenkit Wetting Mechanism Enables Species-Specific Tunable  
1026 Pollen Adhesion, Langmuir, 29, 3012-3023, 10.1021/la305144z, 2013.
- 1027 Longo, A. F., Ingall, E. D., Diaz, J. M., Oakes, M., King, L. E., Nenes, A., Mihalopoulos, N., Violaki, K.,  
1028 Avila, A., Benitez-Nelson, C. R., Brandes, J., McNulty, I., and Vine, D. J.: P-NEXFS analysis of aerosol  
1029 phosphorus delivered to the Mediterranean Sea, Geophysical Research Letters, 41, 4043-4049,  
1030 10.1002/2014GL060555, 2014.
- 1031 Möhler, O., DeMott, P. J., Vali, G., & Levin, Z.: Microbiology and atmospheric processes: the role of  
1032 biological particles in cloud physics., Biogeosciences, 4, 1059-1071, 2007.
- 1033 Morris, C. E., Conen, F., Alex Huffman, J., Phillips, V., Poschl, U., and Sands, D. C.: Bioprecipitation: a  
1034 feedback cycle linking earth history, ecosystem dynamics and land use through biological ice nucleators  
1035 in the atmosphere, Glob Chang Biol, 20, 341-351, 10.1111/gcb.12447, 2014.
- 1036 Muller, S., and Nebe-von-Caron, G.: Functional single-cell analyses: flow cytometry and cell sorting of  
1037 microbial populations and communities, FEMS Microbiol Rev, 34, 554-587, 10.1111/j.1574-  
1038 6976.2010.00214.x, 2010.
- 1039 Myriokefalitakis, S., Nenes, A., Baker, A. R., Mihalopoulos, N., and Kanakidou, M.: Bioavailable  
1040 atmospheric phosphorous supply to the global ocean: a 3-D global modeling study, Biogeosciences, 13,  
1041 6519-6543, 10.5194/bg-13-6519-2016, 2016.
- 1042 Nir, R., Yisraeli, Y., Lamed, R., & Sahar, E.: Flow cytometry sorting of viable bacteria and yeasts  
1043 according to beta-galactosidase activity, Applied and environmental microbiology, 56, 3861-3866, 1990.
- 1044 Oliveira, M., Ribeiro, H., Delgado, J. L., and Abreu, I.: The effects of meteorological factors on airborne  
1045 fungal spore concentration in two areas differing in urbanisation level, Int J Biometeorol, 53, 61-73,  
1046 10.1007/s00484-008-0191-2, 2009.
- 1047
- 1048 Ortiz-Martínez, Mario G., Rosa I. Rodríguez-Cotto, Mónica A. Ortiz-Rivera, Cedric W. Pluguez-Turull,  
1049 and Braulio D. Jiménez-Vélez. Linking endotoxins, African dust PM10 and asthma in an urban and rural  
1050 environment of Puerto Rico. *Mediators of inflammation* 2015.



- 1051 Pérez, C. F., Gassmann, M. I., and Covi, M.: An evaluation of the airborne pollen–precipitation  
1052 relationship with the superposed epoch method, *Aerobiologia*, 25, 313–320, 10.1007/s10453-009-9135-5,  
1053 2009.
- 1054 Pöhlker, C., Huffman, J. A., Förster, J. D., and Pöschl, U.: Autofluorescence of atmospheric bioaerosols:  
1055 spectral fingerprints and taxonomic trends of pollen, *Atmospheric Measurement Techniques*, 6, 3369–  
1056 3392, 10.5194/amt-6-3369-2013, 2013.
- 1057 Pöhlker, C., Huffman, J. A., and Pöschl, U.: Autofluorescence of atmospheric bioaerosols – fluorescent  
1058 biomolecules and potential interferences, *Atmospheric Measurement Techniques*, 5, 37–71, 10.5194/amt-  
1059 5-37-2012, 2012.
- 1060 Pöschl, U.: *Atmospheric Aerosols: Composition, Transformation, Climate and Health Effects*,  
1061 *Angewandte Chemie International Edition*, 44, 7520–7540, 10.1002/anie.200501122, 2005.
- 1062 Rödiger, S., Ruhland, M., Schmidt, C., Schröder, C., Grossmann, K., Böhm, A., Nitschke, J., Berger, I.,  
1063 Schimke, I., and Schierack, P.: Fluorescence Dye Adsorption Assay to Quantify Carboxyl Groups on the  
1064 Surface of Poly(methyl methacrylate) Microbeads, *Analytical Chemistry*, 83, 3379–3385,  
1065 10.1021/ac103277s, 2011.
- 1066 S.-L. Von der Weiden, F. D., and S. Borrmann: Particle Loss Calculator - a new software tool for the  
1067 assessment of the performance of aerosol inlet systems, *Atmospheric Measurement Techniques*, 2, 479–  
1068 494, 2009.
- 1069 Saari, S., Reponen, T., and Keskinen, J.: Performance of Two Fluorescence-Based Real-Time Bioaerosol  
1070 Detectors: BioScout vs. UVAPS, *Aerosol Science and Technology*, 48, 371–378,  
1071 10.1080/02786826.2013.877579, 2014.
- 1072 Šantl-Temkiv, T., Amato, P., Gosewinkel, U., Thyraug, R., Charton, A., Chicot, B., Finster, K., Bratbak,  
1073 G., and Löndahl, J.: High-Flow-Rate Impinger for the Study of Concentration, Viability, Metabolic  
1074 Activity, and Ice-Nucleation Activity of Airborne Bacteria, *Environmental Science & Technology*, 51,  
1075 11224–11234, 10.1021/acs.est.7b01480, 2017.
- 1076 Savage, N. J., Krentz, C. E., Könemann, T., Han, T. T., Mainelis, G., Pöhlker, C., and Huffman, J. A.:  
1077 Systematic characterization and fluorescence threshold strategies for the wideband integrated bioaerosol  
1078 sensor (WIBS) using size-resolved biological and interfering particles, *Atmospheric Measurement  
1079 Techniques*, 10, 4279–4302, 10.5194/amt-10-4279-2017, 2017.
- 1080 Siljamo, P., Sofiev, M., Severova, E., Ranta, H., Kukkonen, J., Plevova, S., Kubin, E., and Minin, A.:  
1081 Sources, impact and exchange of early-spring birch pollen in the Moscow region and Finland,  
1082 *Aerobiologia*, 24, 211–230, 10.1007/s10453-008-9100-8, 2008.
- 1083 Sullivan, S. C., Hoose, C., Kiselev, A., Leisner, T., and Nenes, A.: Initiation of secondary ice production  
1084 in clouds, *Atmos. Chem. Phys. Discuss.*, 2017, 1–22, 10.5194/acp-2017-387, 2017.
- 1085 Taylor, P. E., Jacobson, K. W., House, J. M., and Glover, M. M.: Links between pollen, atopy and the  
1086 asthma epidemic, *Int Arch Allergy Immunol*, 144, 162–170, 10.1159/000103230, 2007.
- 1087 Toprak, E., and Schnaiter, M.: Fluorescent biological aerosol particles measured with the Waveband  
1088 Integrated Bioaerosol Sensor WIBS-4: laboratory tests combined with a one year field study,  
1089 *Atmospheric Chemistry and Physics*, 13, 225–243, 10.5194/acp-13-225-2013, 2013.





- 1090 Van Dilla, M. A., Langlois, R. G., Pinkel, D., Yajko, D., & Hadley, W. K.: Bacterial characterization by  
1091 flow cytometry., *Science*, 220, 620-622, 1983.
- 1092 Wang, Y., Hammes, F., De Roy, K., Verstraete, W., and Boon, N.: Past, present and future applications of  
1093 flow cytometry in aquatic microbiology, *Trends Biotechnol*, 28, 416-424, [10.1016/j.tibtech.2010.04.006](https://doi.org/10.1016/j.tibtech.2010.04.006),  
1094 2010.
- 1095 Wu, Y.-H., Chan, C.-C., Rao, C. Y., Lee, C.-T., Hsu, H.-H., Chiu, Y.-H., and Chao, H. J.: Characteristics,  
1096 determinants, and spatial variations of ambient fungal levels in the subtropical Taipei metropolis,  
1097 *Atmospheric Environment*, 41, 2500-2509, [10.1016/j.atmosenv.2006.11.035](https://doi.org/10.1016/j.atmosenv.2006.11.035), 2007.
- 1098 Yu, X., Wang, Z., Zhang, M., Kuhn, U., Xie, Z., Cheng, Y., Pöschl, U., and Su, H.: Ambient  
1099 measurement of fluorescent aerosol particles with a WIBS in the
- 1100 Yangtze River Delta of China: potential impacts of combustion-related aerosol particles, *Atmospheric  
1101 Chemistry and Physics*, 16, 11337-11348, [10.5194/acp-16-11337-2016](https://doi.org/10.5194/acp-16-11337-2016), 2016.
- 1102 Yue, S., Ren, H., Fan, S., Sun, Y., Wang, Z., and Fu, P.: Springtime precipitation effects on the  
1103 abundance of fluorescent biological aerosol particles and HULIS in Beijing, *Sci Rep*, 6, 29618,  
1104 [10.1038/srep29618](https://doi.org/10.1038/srep29618), 2016.
- 1105 Yue, S., Ren, H., Fan, S., Wei, L., Zhao, J., Bao, M., Hou, S., Zhan, J., Zhao, W., Ren, L., Kang, M., Li,  
1106 L., Zhang, Y., Sun, Y., Wang, Z., and Fu, P.: High Abundance of Fluorescent Biological Aerosol  
1107 Particles in Winter in Beijing, China, *ACS Earth and Space Chemistry*, 1, 493-502,  
1108 [10.1021/acsearthspacechem.7b00062](https://doi.org/10.1021/acsearthspacechem.7b00062), 2017.
- 1109 Zhen, H., Han, T., Fennell, D. E., and Mainelis, G.: Release of free DNA by membrane-impaired bacterial  
1110 aerosols due to aerosolization and air sampling, *Appl Environ Microbiol*, 79, 7780-7789,  
1111 [10.1128/AEM.02859-13](https://doi.org/10.1128/AEM.02859-13), 2013.
- 1112 Ziemba, L. D., Beyersdorf, A. J., Chen, G., Corr, C. A., Crumeyrolle, S. N., Diskin, G., Hudgins, C.,  
1113 Martin, R., Mikoviny, T., Moore, R., Shook, M., Thornhill, K. L., Winstead, E. L., Wisthaler, A., and  
1114 Anderson, B. E.: Airborne observations of bioaerosol over the Southeast United States using a Wideband  
1115 Integrated Bioaerosol Sensor, *Journal of Geophysical Research: Atmospheres*, 121, 8506-8524,  
1116 [10.1002/2015JD024669](https://doi.org/10.1002/2015JD024669), 2016.  
1117



1 **Table 1:** Summary of the SpinCon II sampling events, the 24 h. averaged RH, ambient temperature, the  
 2 assigned meteorological category (using Section 4.4 definitions) and the corrected FCM-derived PBAP  
 3 number concentration (1 to 5  $\mu\text{m}$ ) for each sample collected during this study.

4

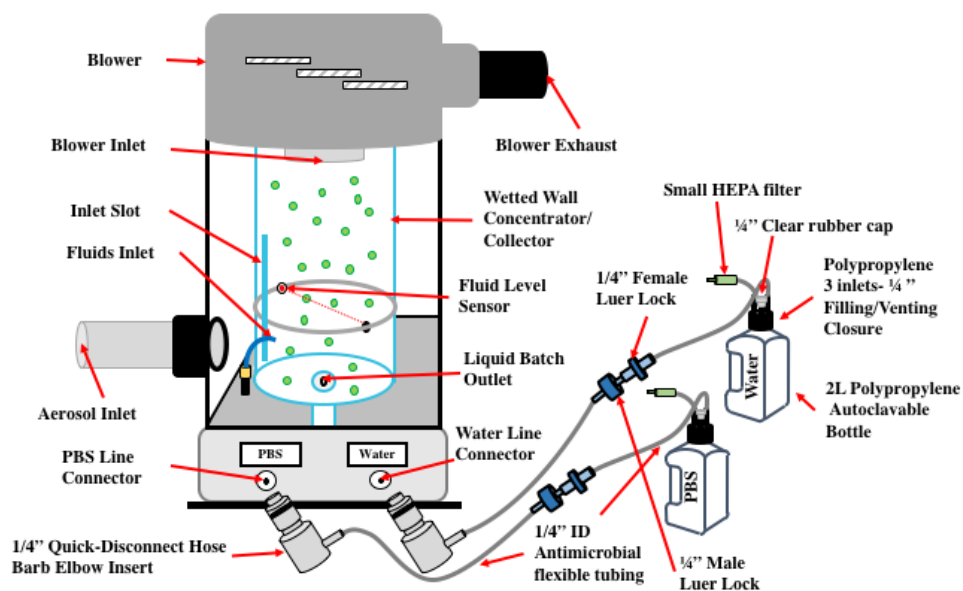
5

Date (starting – ending time)	RH (%)	Temperature (°C)	Meteorological Category	PBAP Concentration ( $\text{m}^{-3}$ ) 1 to 5 $\mu\text{m}$ diameter range
4/7/15 (11:17 - 15:17) *	70.9	21.4	Humid, Warm	$9.282 \times 10^4$
4/8/15 (11:10 - 15:10)	53.6	24.9	Dry, Warm	$5.203 \times 10^5$
4/9/15 (11:15 - 15:15)	53.8	25.3	Dry, Warm	$1.254 \times 10^5$
4/14/15 (11:30 - 15:30) *	76.8	22.5	Humid, Warm	$8.253 \times 10^4$
4/15/15 (11:40 - 15:40) *	83.6	18.9	Humid, Warm	$1.234 \times 10^5$
4/16/15 (10:55 - 14:55)	86.3	12.5	Humid, Cold	$3.399 \times 10^5$
4/21/15 (13:15 - 17:15)	43.2	16.6	Dry, Cold	$4.741 \times 10^5$
4/22/15 (11:25 - 15:25)	41.2	19.0	Dry, Warm	$3.351 \times 10^5$
4/23/15 (11:35 - 15:35)	48.1	16.8	Dry, Cold	$1.708 \times 10^6$
4/28/15 (12:25 - 16:25)	45.3	17.0	Dry, Cold	$4.899 \times 10^5$
4/29/15 (11:55 - 15:55) #	79.4	14.2	Humid, Cold	$4.591 \times 10^5$
4/30/15 (12:10 - 16:10)	57.3	17.4	Dry, Cold	$9.603 \times 10^5$
5/13/15 (10:50 - 14:50)	40.1	23.5	Dry, Warm	$3.680 \times 10^5$
5/14/15 (11:50 - 15:50)	52.3	23.0	Dry, Warm	$4.851 \times 10^5$
5/15/15 (10:19 - 14:19)	64.4	23.1	Dry, Warm	$1.656 \times 10^6$

6 \* Sampling occurred post-rain event.

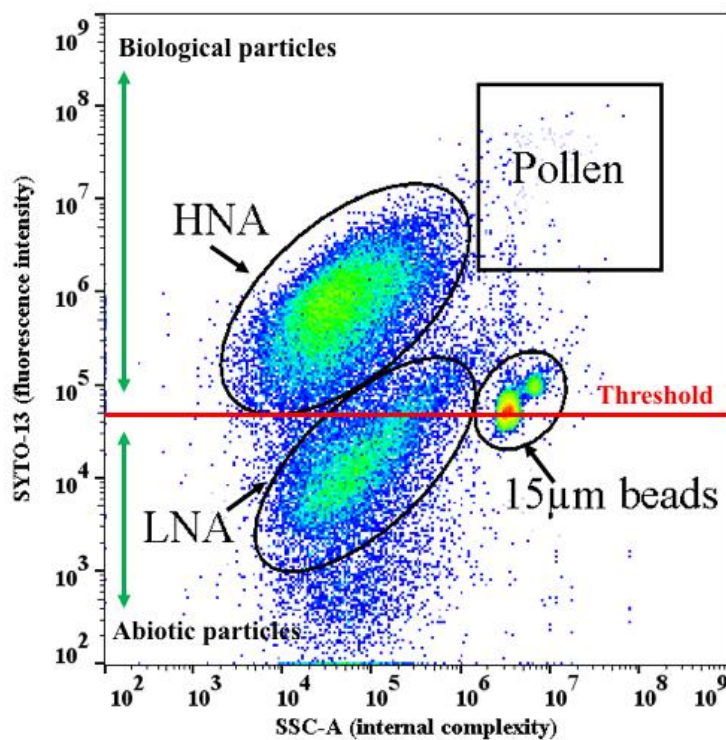
7 # Sampling occurred during a rain event.

8



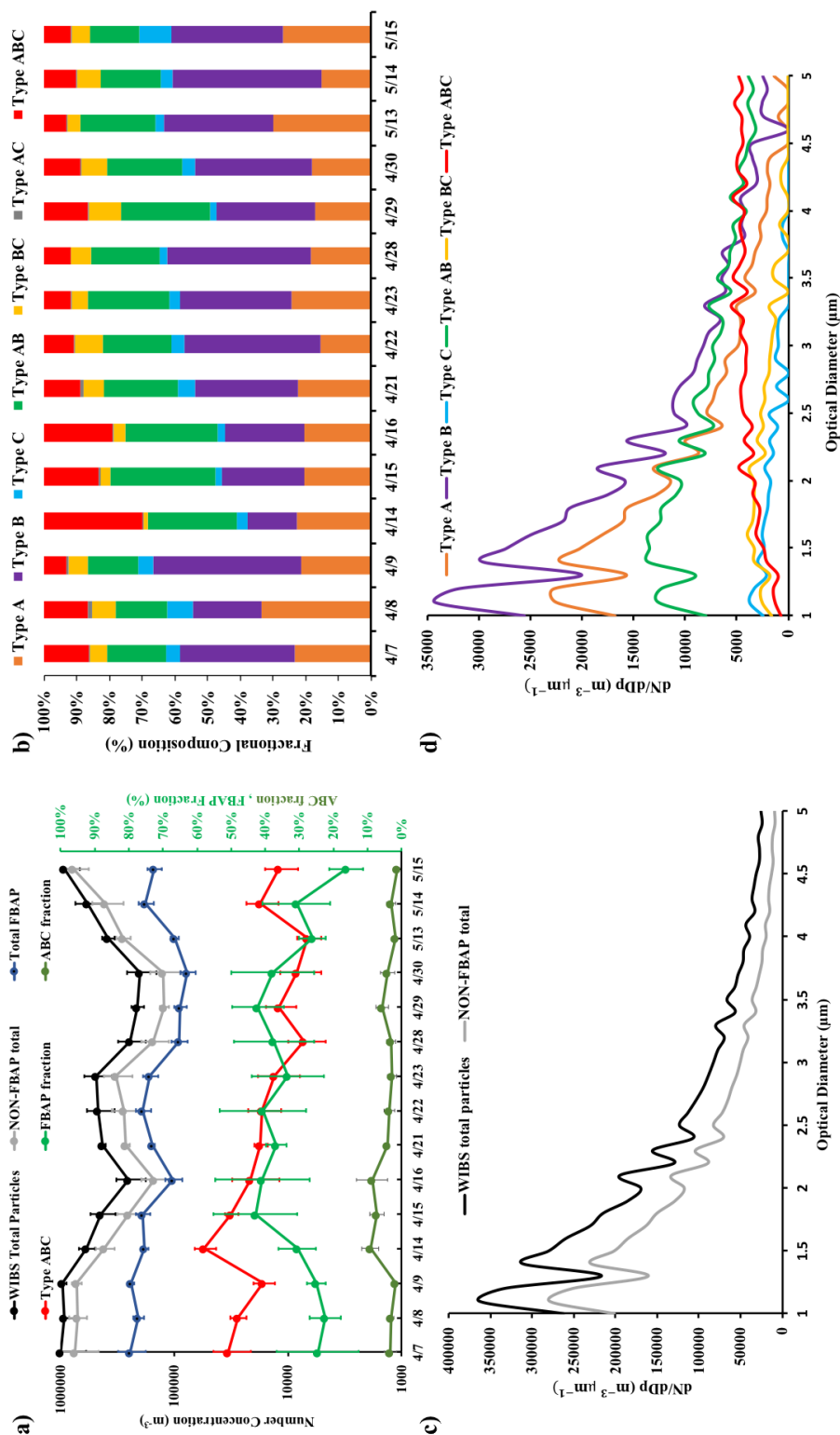
9  
10  
11  
12

**Figure 1:** SpinCon II sampling setup including modified fluid supply system with anti-microbial tubing and 2L Autoclavable bottles.



13  
14  
15  
16  
17  
18  
19

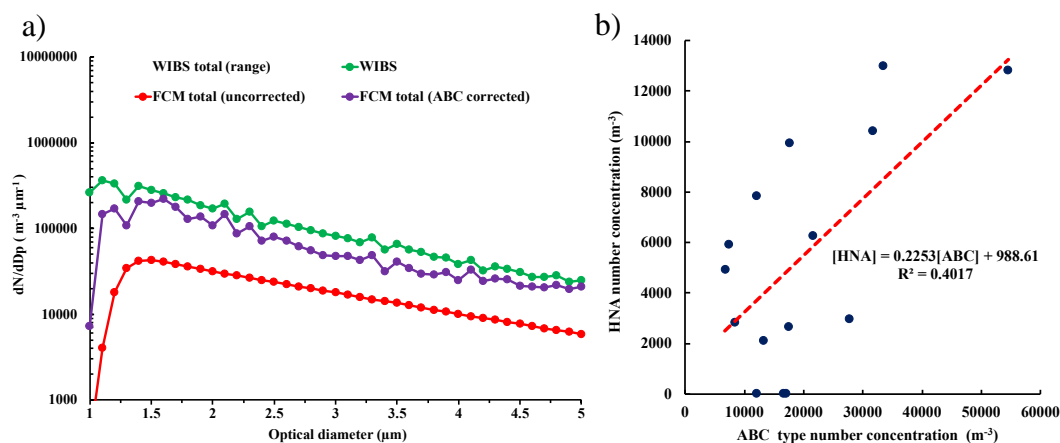
**Figure 2:** FL1-A vs. SSC-A plot used to identify populations in collected rooftop atmospheric samples (April 14, 2015 4hr sample) including: the 42k threshold line in red and, abiotic particles (below threshold) and biological particles (above threshold) designated regions. The fraction of the LNA population above the threshold line is referred as the “bioLNA” population.



20  
 21 **Figure 3:** WBS-4A 4h averaged results of WBS total particle, NON-FBAP, total FBAP and type ABC concentrations in the left Y-axis and ABC  
 22 and FBAP fraction in the right Y-axis in (a) and FBAP types number concentration fractional composition in (b); and average 1 to 5  $\mu\text{m}$  size  
 23 distributions (average of the 15 sampling events 4h average) over the 15 SpinCon II sampling events of WBS total particles and NON-FBAP in (c)  
 24 and all FBAP types, except AC type in (d). AC type showed low statistics and constituted less than 1% of the total FBAP (not shown)



25  
26



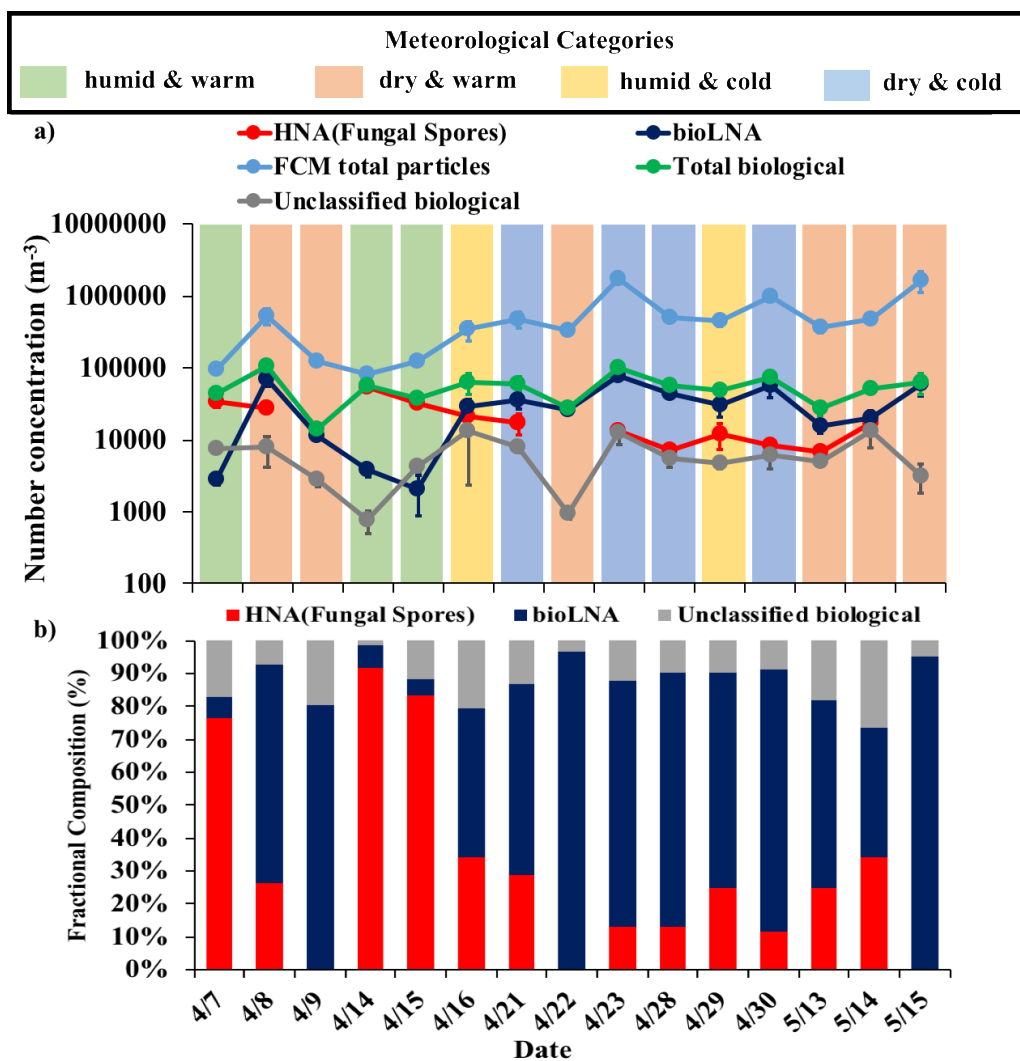
27  
28  
29  
30  
31  
32  
33  
34

**Figure 4:** WBS-4A, FCM uncorrected and FCM (ABC corrected) total particle concentration (1 to 5  $\mu m$ ) average size distributions (geometrically averaged over the 15 SpinCon II sampling events) including WBS range ( $\pm$  geometric standard deviation factor) in (a); and HNA and ABC type concentration correlation in the 1 to 5  $\mu m$  range in (b) including it linear correlation in red.





35  
 36

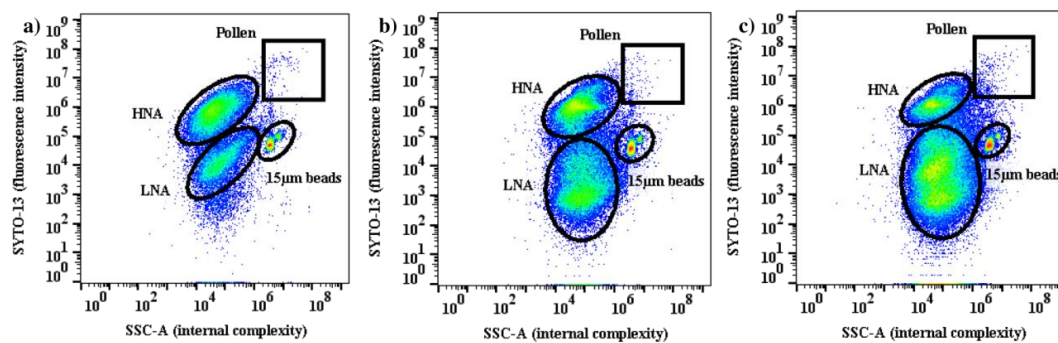


37  
 38  
 39  
 40  
 41  
 42  
 43  
 44  
 45  
 46  
 47  
 48  
 49

**Figure 5:** FCM total particle, HNA, bioLNA and total PBAP number concentrations in the 1 to 5 $\mu$ m range highlighting the prevailing meteorological category during each sampling event in (a); HNA and bioLNA number concentration fractional compositions for each sampling event in (b).



50  
51  
52  
53  
54

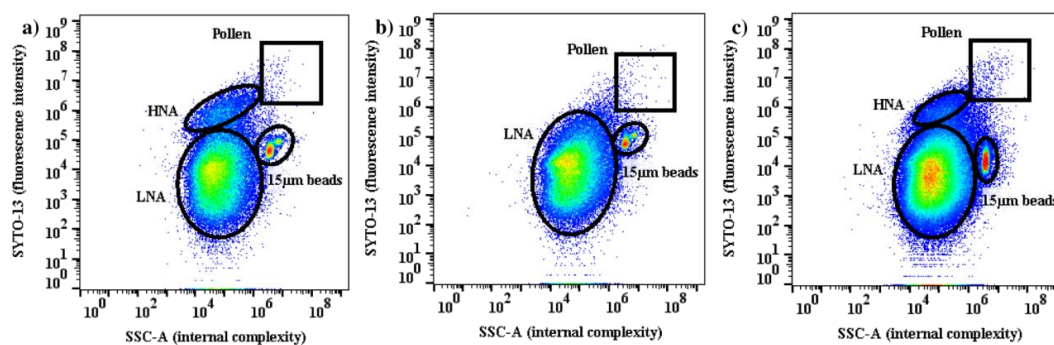


55  
56  
57  
58  
59  
60  
61  
62  
63

**Figure 6:** FL1-A vs. SSC-A FSC plots for (a) April 14, (b) April 15, and, (c) April 16. This period was characterized by a transition from humid & warm to humid & cold conditions (diurnal average RH=77%, T=22.5 °C on 4/14; RH=84%, T=18.9 °C on 4/15, and RH= 86%, T= 12.5 °C on 4/16). The FCM plots during this transition period show a decrease of fungal population and an increase of the LNA population. In each population, warmer colors represent higher particle concentrations.



64



65

66

67

68

69

70

71

**Figure 7:** Similar to Figure 6, but for (a) April 21, (b) April 22, (c) April 23, which was characterized by dry and variability in temperature (diurnal average RH=43%, T=16.6 °C on 4/21; RH=41%, T=19.0 °C on 4/22, and, RH= 48%, T= 16.8 °C on 4/23). Note the disappearance of the fungal spore population on the warmest day (4/22).

72

73

74

75

76

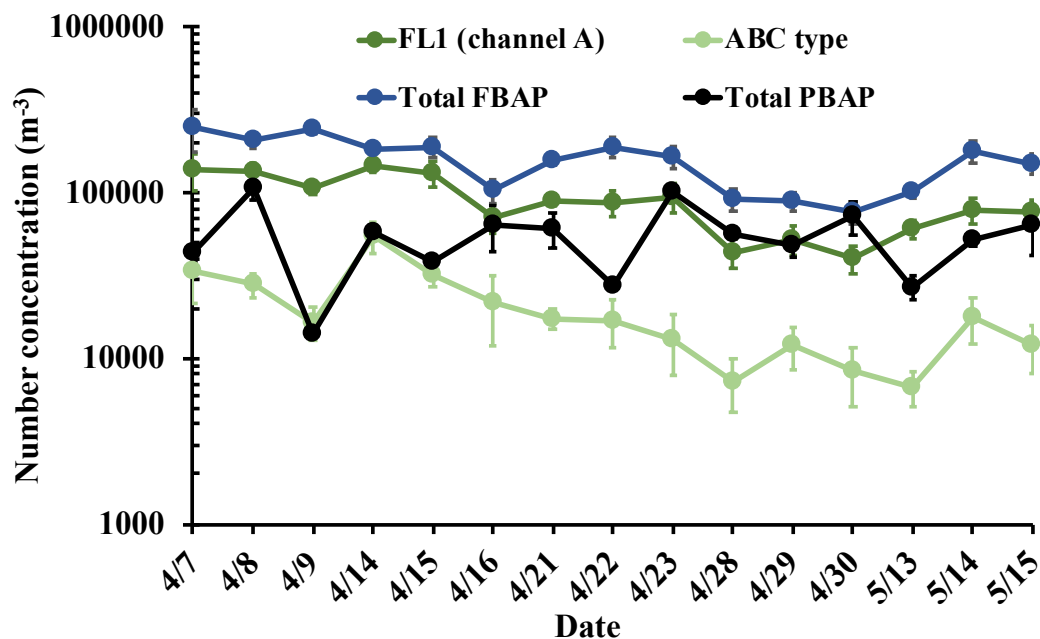
77

78

79

80

81



82  
83

84 **Figure 8:** WIBS-4A total FBAP, FL1 and ABC type, and FCM total particle number concentrations in  
85 the 1 to 5 $\mu$ m range for each sampling event from April 7 to May 15, 2015.

86  
87  
88  
89

90  
91  
92  
93  
94